MODELLING OF THERMAL DEBINDING STEP IN METAL INJECTION MOULDING

TINNAPHOP POOLKHAOLAN

A THESIS SUBMITTED IN PARTIAL FULFILLMENT

OF THE REQUIREMENT FOR THE DEGREE OF

MASTER OF ENGINEERING IN AUTOMOTIVE ENGINEERING

(INTERNATIONAL PROGRAM)

INTERNATIONAL COLLEGE

KING MONGUT'S INSTITUTE OF TECHNOLOGY LADKRABANG

2013

KMITL- 2013-IC-M-004-025

Thesis title	Modelling of Thermal Debinding Step in Metal Injection Moulding
Student name	Mr. Tinnaphop Poolkhaolan
Student ID	51061907
Degree	Master of Engineering
Program	AUTOMOTIVE ENGINEERING
Year	2009
ADVISOR	Assoc. Prof. Dr. Jarruwat Charoensuk
	Dr. Anchalee Manonukul
	Assoc. Prof. Dr. Kunio Takahashi

ABSTRACT

Metal injection moulding process is a near-net-shape manufacturing process for small parts used in various industries including automobile, electrical and electronic. It consists of four main steps, namely mixing, injection, debinding and sintering. In the debinding step, the binder, a multi-component of polymeric components, in a specimen can be removed by several debinding methods, e.g. thermal debinding, solvent debinding, and wicking debinding. Thermal debinding is the most common process for mass products. Nevertheless, it is the most time-consuming step. The deformation of a specimen could occur because of the usage of high heating rate to reduce the total debinding time. Therefore, the low heating rate is currently employed. The trial-and-error experiments were used to determine the proper heating rate without any deflects. This work assessed the model developed by the general-purpose software to investigate the important parameter throughout of thermal debinding. The user-defined function based on thermal degradation of polypropylene binder, were coded tembedded into Ansys Fluent. The weights of binder which remain in the specimen were forecasted. The validation were performed experimentally that showed good agreement. In addition, internal pressure were studied that could induce the deflect to the specimen. Moreover, the model was used to provide the newly heating profile for reduction the debinding time. The recommended heating profile is divided into two heating regimes. The first regime should be a heating rate of 0.2 °c/min with the duration of 42,000 seconds. The second regime should be a heating rate of 1 c°/min with the duration of 13,000 seconds.

ACKNOWLEDGEMENTS

This thesis could not be completed without the assistance of many person to whom I would like to express my sincere appreciation.

First of all, I would like to express my deep gratitude and appreciation to Dr. Anchalee Manonukul at National Metal and Materials Technology Center (MTEC) and Assoc. Prof. Dr. Jarruwat Charoensuk at King Mongkut's Institute of Technology Ladkrabang (KMITL), my great advisors for their best support, valuable time, and criticism and always give their advices from the beginning up to the end, so that I could be able to accomplish this thesis as a partial fulfillment. Without their helpful, I would not be able to get knowledge, experiences, and be able to complete my thesis. This dissertation also would not be possible without the help of many people at MTEC and KMITL who always cheer up me to pass many situations that would make me to success for today.

I would like to thank you for, MTEC who provide support for Ansys Fluent which is very important and useful program for me to complete my thesis topic. Furthermore, I would like to thank you for kindness of staffs at this center that always help me with their advices, materials and encouragements. I also would like to give special thanks to my supervisors at my current job who understand, share their experiences and help to ensure that my work and my study will go as smooth as possible. Moreover, I would like to thank Mr. Niwat Phoocharoen at KMITL for well suggestion for simulation skill.

In this very special moment, I would like to express my deepest thanks for my beloved family who always understand and take care of me and provide every support for my work and study, especially my super mom, for her love encouragement and her spirit that made me possible to finish my study. Last but not least, I would like to thank my friends who also beside me and give their moral supports, concern, love and inspiration during my study time.

Tinnaphop Poolkhaolan

CONTENTS

Page

CONTENTS (CONT.)

Page

LIST OF TABLES

LIST OF FIGURES

LIST OF FIGURES (CONT.)

LIST OF FIGURES (CONT.)

Figure Page

Chapter 1

INTRODUCTION

1.1 Introduction

Metal injection moulding process is a near-net-shape manufacturing process for automotive parts. It consists of four main steps, mixing, and injection, debinding and sintering. Metal powder and binder are mixed together and become feedstock in the mixing step. The feedstock is injected into the near-net-shape part, namely a green part, in the injection step. The binder in the green part is removed in the debinding step. The final step is sintering where metal powder is heated up to high temperature to join the powder together. To increase productivity of MIM can be performed by reducing production time in debinding step, the most-time consuming.

1.2 Background and Problem Statement

In the debinding step, the binder, a multi-component system containing the backbone polymer, surfactant, and plasticiser, is removed out of the specimen. There are several debinging methods for example thermal debinding, solvent debinding, and wicking debinding. Thermal debinding is the suitable process to produce mass products; nevertheless, it is the most time-consuming step. As the temperature is increased, the mechanisms of heat and mass transfer in porous media such as phase transformation, mass convection and diffusion of liquid and gas phase occur in the specimen. The thermal debinding is divided into two stages. The first stage is the removal of surfactant and plasticiser, which are the low-molecular-weight component, and the second stage is the removal of backbone polymer, which is the high-molecular-weight component. The reduction of total debinding time is the usage of high heating rate that can lead to defects such as swell and crack on the specimen. Therefore, the time-consuming and trial-and-error experiments are required to optimise the appropriate heating rate. The numerical simulation can be adopted to study phenomena during thermal debinding. The heat and mass transfer inside the specimen can be investigated based on a simulation model. The reduction of time can be archived with the model of thermal debinding which is useful for improvement of the debinding time.

1.3 Objective of The Study

1. This work will focus on the development of thermal debinding model on a platform of a general-purpose software. The model and numerical results will be validated with the experimental results.

2. The model will be used to investigate the importance of properties that can damage the specimen throughout the second stages of thermal debinding.

3. The model is used as basic for newly proposed heating profile for the second stage of thermal debinding

1.4 Scope of the Study

There are various phenomena inside the specimen during thermal debinding. The heat and mass transfer occur in the specimen which will be transformed to porous medium. The cause of deflection of the specimen will be limited to internal pressure in the specimen. High heating rate will be used for thermal debinding to monitor swelling or distortion of the specimen shape. The single phase simulation model with rigid body assumption will be compared with the experimental result of various heating rates. Finally, the model will be used to provide recommendation of the proper heating profile for thermal debinding.

1.5 Methodology

The model of thermal debinding will be developed based on thermal degradtion of polymer to forecast mass reduction rate of thermal debinding. The computer code will be embedded to CFD commercial program Ansys Fluent to modify the default model for thermal degradation of polymer binder. The thermogravimetric analysis will be used for finding out parameters for thermal degradation mechanisms which is coded for the mass source in Ansys Fluent. The experiment will be done to validate the model for various heating rate. There will be the heating rate that safe the specimen from any damage. Then, the newly heating profile will be performed based on the safe heating rates.

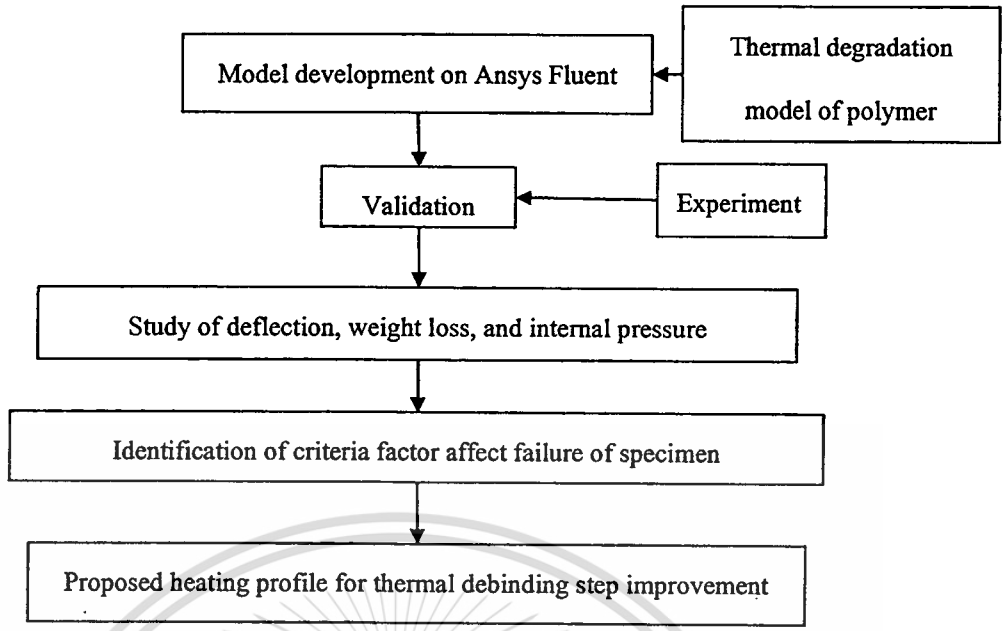

Figure 1.1 flow chart of methodology

Chapter 2

LITERATURE REVIEW AND THEORY

2.1 Early research.

The removal of binder in thermal debinding step behaves like the heat and mass transfer in porous media. In this work, the multi-component binder will be heated up in the furnace. The temperature on the outer surface are equal to the ambient temperature. The mechanisms of binder removal during the thermal debinding are phase transition, convection, diffusion, and heat transfer in porous media.

In the first stage, the low-molecular-weight component melts from solid to liquid phase and vaporised inside the specimen and is carried by the inert gas such as argon gas at the outer surface. On the other hand, the high-molecular-weight component melts also from solid to liquid phase. In the second stage, the liquid of high-molecular-weight component degrades to liquid volatile fragment and the liquid volatile fragment evaporates and diffuses to the outer surface (Barone and Ulicny, 1990). The model for the removal of the binder will be the multi-phase flow in porous media modelling. The governing equations are the continuity equations for multiphase, the energy equation, and the momentum equation. The weight loss will be monitored for validation.

There were numerical models adopted to simulate the thermal debinding process. The thermal debinding of one component binder was modelled and the gas transport was the main mechanism during the step based on the liquid-gas interface assumption (Calvert and Cima, 1990). The gas pressure of degraded liquid polymer was controlled below the atmosphere pressure to prevent the bubble formation (Maximenko and Van der biest, 1998). The numerical and experimental results showed that there was no liquid-gas interface in thermal debinding step of the specimen that consisted of both low-molecular-weight and high-molecular-weight component (Lewis and Galler, 1996). There were also the models predicted the removal of the low-molecular-weight component in the first stage of thermal debinding and the results showed that effect of capillary flow of liquid phase was important (Barone and Ulicny, 1990). The models of two-component binder were investigated throughout both stages of the thermal debinding.

There were several mass transport mechanisms such as liquid flow, gas flow, convection, and diffusion. Moreover, the numerical result was in good agreement with the experimental result (Khoong, Lam, and et al., 2010). The existing models were useful to validate and predict the thermal debinding by the numerical algorithm of the individual authors. In addition, the models were analysed on the simple specimen. The model for general usage is still not introduced.

2.2 Polymer degradation

Thermal degradation is a phenomenon of polymeric material transformation at high temperature condition. The polymer consists of monomer chains. They are dent in form of solid. During absorption of thermal energy, solid polymer melts into liquid polymer. The chains are not stable with losing their bond between chain. Therefore, polymer become to liquid under melting process. Then the liquid decompose to volatile fragment and evaporate to vapor.

2.2.1 Kinetic parameters of Thermo-gravimetic analysis

For thermal degradation of polymer, a rate of reaction can be expressed as a product of a temperature-dependent function (Chan and Balke, 1997).

$$\frac{dW}{dt} = AW^n \exp(-\frac{E}{RT}) \quad \text{..... (1)}$$

or

$$\ln(\frac{dW}{dt}) = \ln A + n\ln W - \frac{E}{RT} \quad \text{..... (2)}$$

where w is the weight fraction remaining in a TGA run, A is the pre-exponential factor, n is reaction order, E is an activation energy, R is the universal gas constant, and T is absolute temperature.

There are a few methods to obtain the kinetic parameters such as the activation energy (E), a reaction order, and pre-exponential factor. The first method is single heating rate using one constant heating of TGA. The second is multiple heating rates (Chan and Balke, 1997).

The conventional approach to obtain the kinetic parameters is using one constant heating rate since it is a cost-less method. It can provide the reaction order (n) and the activation energy (E).

The difference form of (1) at different temperatures is

$$\Delta \ln r = n\Delta \ln W - (\frac{E}{R})\Delta(\frac{1}{T}) \quad \text{..... (3)}$$

Dividing (3) by $\Delta(\frac{1}{T})$ gives

$$\frac{\Delta \ln r}{\Delta(1/T)} = n\frac{\Delta \ln W}{\Delta(1/T)} - \frac{E}{R} \quad \text{..... (4)}$$

Thus, a plot of $\frac{\Delta \ln r}{\Delta(1/T)}$ versus $\frac{\Delta \ln W}{\Delta(1/T)}$ should be a straight line with slope equal to the order of reaction n and an intercept of $-\frac{E}{R}$

Then divide (4) by $\Delta \ln W$ gives

$$\frac{\Delta \ln r}{\Delta \ln W} = n + E\left(-\frac{\Delta(1/T)}{R\Delta \ln W}\right) \quad \text{..... (5)}$$

a plot of $\frac{\Delta \ln r}{\Delta \ln W}$ versus $-\frac{\Delta(1/T)}{R\Delta \ln W}$ should also be a straight line of slop E and an intercept n.

By assuming that the order of reaction n is constant, then (2) may be rearranged as follows:

$$(\ln r - n \ln W) = E\left(-\frac{1}{RT}\right) + \ln A \quad \text{..... (6)}$$

If the activation energy E is assumed to be a constant over a specific temperature range, then the slope over this range of plot of $\ln r - n \ln W$ versus $-\frac{1}{RT}$ should be equal to the activation energy E.

2.2.2 Thermal dedinding of polymeric binder

A binder is polymeric compound. It helped forming the shape of specimen. Binder system consists of surfactant lubricant and backbone polymer. The surfactant helps powder and binder mixed homogeneously. The lubricant gives flow ability during mixing step and injection step.

In debinding step of MIM process, thermal debinding is the most conventional method to remove the binder blend out of the injected part. Because of heated air, thermal debinding can be a cheapest route. Moreover, more numbers of parst can be debinded in the one batch.

In a furnace, MIM parts are heated by hot air flow. Phase transforms of the polymer in binder continue as the temperature increases. The degradation reaction occurs during the process. Oxygen in air diffuses to specimen causing degradation reaction. Therefore, thermal debinding is considered to be a oxidative degradation.

2.3 Computational fluid dynamics

Computational fluid dynamics of CFD is the analysis of systems involving fluid flow, heat transfer and associated phenomena such as chemical reactions. Applications of CFD are used in various industrial areas. Some examples are:

-Aerodynamics of aircraft and vehicles: lift and drag

-Power plant: combustion in internal combustion engines and gas turbines

-Chemical process engineering: mixing and separation, polymer moulding

It is well-known that computer simulation is the cost-effective tools. it is very cheap to study parameters instead of try-out-error experiments. Large volumes of results can be virtualised with no added costs. In addition, the optimisation can be conducted to find out the important performance of the solution.

CFD codes in general-proposed softwares like Ansys Fluent contain three main elements: a pre-processor, a solver, and a post-processor. Each element is detailing in next section

Pre-processor

This stage is a preparing of necessary inputs to a CFD program via user-interface of commercial CFD packages. User inputs involve data of flow problem such as:

-Geometry of region of interest called the computational domain

-Meshing-the sub-division of the domain into a number of smaller portion call meshes or cells

-Physical and chemical phenomena that need to be modelled

-Definition of fluid properties

-Boundary condition setting up

Solver

CFD Ansys Fluent utilises the finite volume method, a special finite difference formulation. The numerical algorithm includes a few steps:

-Integration of the governing equations of fluid flow over all domain

-Discretisation-conversion of the resulting integral equations into a system of algebraic equations

-Solution of the algebraic equation by an iterative method

The conservation of flow variables ϕ, e.g. mass, momentum, and energy, in finite controlled volume is balanced for all domain. That can be expressed as

$$\left\{\begin{array}{c}\text{Rate of change}\\ \text{of } \phi \text{ in the}\\ \text{control volume}\\ \text{with respect to}\\ \text{time}\end{array}\right\}+\left\{\begin{array}{c}\text{Net rate of}\\ \text{increase of}\\ \phi \text{ due to}\\ \text{convection into}\\ \text{the control volume}\end{array}\right\}=\left\{\begin{array}{c}\text{Net rate of}\\ \text{increase of}\\ \phi \text{ due to}\\ \text{diffusion into}\\ \text{the control}\\ \text{volume}\end{array}\right\}+\left\{\begin{array}{c}\text{Net rate of}\\ \text{creation of}\\ \phi \text{ inside}\\ \text{the control volume}\end{array}\right\}$$

All variable in a control volume are conserve variables. Transport phenomena for each control volume is transient, convection, diffusion, and source. Transient relates with rate change of flow variable. The convection is transportation due to fluid flow. The diffusion is transportation due to variation of ϕ between the control volumes. The source involves creation of flow variable in the control volume. The physical phenomena are complex and non-linear so an iterative solution(Gauss-Seidel point iterative techniques, etc.) is required to solve the flow variable over domain.

Post-processor

To illustrate the results in domain, various type of display, showing fluid and other variable flow such as pressure, temperature, velocity, etc., are :

-Vector plots

-Line and contour plots

-2D and 3D surface plots

-Particle tracking

-Other user defined display

2.3.1 The governing equations of fluid flow

Fluid and others properties, flowing in systems of interest, conserve throughout fluid domain., All conservation can express in the governing equation form as

Mass conservation,

$$\frac{\partial \rho}{\partial t}+\nabla\cdot(\rho\vec{v})=0 \quad \text{.....(7)}$$

Momentum conservation,

$$\frac{\partial \rho\vec{v}}{\partial t}+\nabla\cdot(\rho\vec{v}\vec{v})=\nabla p+\left(\mu\ grad\ \vec{v}\right)+s_m \quad \text{.....(8)}$$

Energy conservation,

$$\frac{\partial \rho\vec{v}i}{\partial t}+\nabla\cdot(\rho i\vec{v})=-p\nabla\vec{v}+\nabla\cdot\left(k\ grad\ \vec{v}\right)+s_i \quad \text{.....(9)}$$

where ρ is density of fluid, $\vec{v}$ is velocity, μ is viscosity, s_m is momentum sources, i is internal energy, k is thermal conductivity, and s_i is energy sources.

The governing equations above are concluded in the general form for all variables in flow field. The flow variable (ϕ) is substituted into conservation equation then combine to be a transport equation,

$$\frac{\partial \rho \phi}{\partial t} + \nabla \cdot (\rho \vec{v} \phi) = \nabla \cdot (\Gamma \nabla \phi) + s_{\phi} \quad (10)$$

2.3.2 Flow in porous media

Porous media is a substrate that consists of solid and void. Void in porous material can be fill with gas or liquid. There are two types of void, open pore and close pore. The interconnect helps fluid flow thought the media for open pores type. However, Fluid cannot flow in the close pore type.

MIM part can be considered to be a porous media as the binder is removed out in debinding step. Initially, the green part is the solid that composes of polymeric binder and solid metal. As the binder is burnout, it leaves space in the green part. Air and gas of degradation can flow into the specimen.

To describe flow in porous media, Darcy's law will be conducted to gain how flow fluid flow thought pores network. The Darcy's law explains relation between pressure and velocity of fluid flow as

$$\nabla p = -\frac{\mu}{K} \vec{v} \quad (11)$$

where K is permeability.

For laminar flow, fluid in porous media flows because of pressure difference. Flow ability of fluid in the media is depended on viscosity and permeability. Darcy's law is valid for slow flow though a porous medium with rigid solid matrix.

Porosity is value to define the ratio of volume of void per total volume of system or control volume in CFD analysis. It can be written as

$$\gamma = \frac{V_{void}}{V_{total}} \quad (12)$$

2.3.3 Multiphases flow

In nature, majority of flow character in this particular problem are a mixture of phases. Multiple fluids present in system such as gas, liquid, and solid in various problems of flow. Multiphase flow can be grouped into four categories: gas-liquid or liquid-liquid flows; gas-solid flows; liquid-solid flows; and three-phase flows. In multiphase flow, a general transport equation may be written as

$$\frac{\partial \alpha\rho\phi}{\partial t} + \nabla\cdot(\alpha\rho\vec{v}\phi) = \nabla\cdot\bar{\bar{\tau}} + s_{\phi} \quad (13)$$

where α is the phase volume fraction. ρ is the mixture phase density, ϕ is either a mixture or a phase variable, $\vec{v}$ is the mixture of phase velocity, $\bar{\bar{\tau}}$ is the diffustion term, S_{ϕ} is the source term.

2.3.4 Multiphase flow in porous media

Thermal debinding is a step to remove binder compound from the green part. The thermal energy transfer from heated air to MIM parts in debinding furnace. Temperature of polymeric binder is increased to degradation point. The polymer starts degradation and leaves the part via flowing of volatile vapor. Then, there are small pores created instantly as degradation continues. At degradation temperature, thermal energy is related to the reaction of phase change. Vapour of degraded product increase thoughtout the part as a result of high internal pressure. As the polymer decreases, MIM part transforms from solid to porous material. The porosity also varies during thermal debinding.

The governing equations of thermal debinding step can be written to capture physical phenomena. Adding porosity (γ) to all term in general equation can modify to solve the porous problems.

continuity equation

$$\frac{\partial \alpha\rho_q\phi_q}{\partial t} + \nabla\cdot(\alpha\rho_q\vec{v}_q) = \gamma\sum_{p=1}^{n}\left(\dot{m}_{pq} - \dot{m}_{qp}\right) + \gamma s_{\phi} \quad (14)$$

where γ is porosity, $\vec{v}_q$ is the velocity of phases q and $\dot{m}_{pq}$ characterises the mass transfer from the p^{th} to q^{th} phase, $\dot{m}_{qp}$ is characterises the mass transfer from phase q to phase p and S_q is mass source of phase q.

momentum equation

$$\frac{\partial\left(\gamma\alpha_q\rho_q\vec{v}_q\right)}{\partial t} + \nabla\cdot(\gamma\alpha_q\rho_q\vec{v}_q) =$$
$$-\gamma\alpha_q\nabla p + \nabla\cdot\left(\gamma\bar{\bar{\tau}}_q\right) + \gamma\alpha_q\rho_q\vec{g} + \gamma\sum_{p=1}^{n}\left(\vec{R}_{pq} + \dot{m}_{pq}\vec{v}_{pq} - \dot{m}_{qp}\vec{v}_{qp}\right)$$
$$+\gamma\left(\sum_{p=1}^{n}\left(\dot{m}_{pq} - \dot{m}_{qp}\right)\right) + \gamma\left(\vec{F}_q + \vec{F}_{lift,q} + \vec{F}_{vm,q}\right) + \alpha_q\left(\frac{\mu}{K} + \frac{C_{cp}}{2}\left|\vec{v}_q\right|\right)\vec{v}_q \quad (15)$$

where $\vec{F}_q$ is and external body force, $\vec{F}_{lift,q}$ is a lift force, $\vec{F}_{vm,q}$ is a virtual mass force, $\vec{R}_{pq}$ is and interaction force between phases, p is the pressure shared by all phases, $\vec{v}_{pq}$ and $\vec{v}_{qp}$ are the interphase velocity, and $C_{2\rho}$ is the inertial resistance factor.

For porous media problem, term of $\alpha_q\left(\frac{\mu}{K} + \frac{C_{2\rho}}{2}\left|\vec{v}_q\right|\right)\vec{v}_q$ is added into the equation. It comprises of lamina flow term ($\frac{\mu}{K}$) and turbulence flow term $\frac{C_{2\rho}}{2}\left|\vec{v}_q\right|$.

energy equation for fluid

$$\frac{\partial(\gamma\alpha_q\rho_q h_q)}{\partial t}+\nabla\cdot(\gamma\alpha_q\rho_q\vec{v}_q\bar{h}\,)=$$
$$\gamma\alpha_q\frac{\partial p_q}{\partial t}+\gamma\bar{\bar{\tau}}_q:\nabla\cdot\vec{v}_q-\nabla\cdot(\gamma\vec{q}_q)+\gamma S_q+\gamma\sum_{p=1}^{n}(Q_{pq}+\dot{m}_{pq}h_{pq}-\dot{m}_{qp}h_{qp})+Q_{sp} \quad (16)$$

where h_q is the specific enthalpy of the q^{th} phase, $\vec{q}_q$ is the heat flux, S_q is a source term that includes sources of enthalpy (e.g. due to chemical reaction of radiation), Q_{pq} is the intensity of heat exchange between the p^{th} and q^{th} phases, and h_{pq} is the interphase enthalpy. The heat exchange between phases must comply with the local balance conditions. Q_{sp} is the heat transfer between the solids surface and the phase q in a porous media.

Energy equation for solid

$$\frac{\partial(\gamma\rho_f E_f+(1-\gamma)\rho_s E_s)}{\partial t}+\nabla\cdot(\vec{v}_q(\rho_f E_f+p))=$$
$$S_f^h+\nabla\cdot\left[k_{eff}\nabla T-\left(\sum_i h_i J_i\right)+(\bar{\bar{\tau}}+\vec{v})\right] \quad (17)$$

where E_f is total fluid energy, E_s is total solid medium energy, ρ_f is fluid density, ρ_s is solid medium density , γ is porosity of the medium, k_{eff} is effective thermal conductivity of the medium and S_f^h is fluid enthalpy source term

The effective thermal conductivity in the porous medium, , is computed by Ansys Fluent as the volume average of the fluid conductivity and the solid conductivity.

$$k_{eff}=\gamma k_f+(1-\gamma)k_s \quad (18)$$

Where k_f is fluid phase thermal conductivity and k_s is solid medium thermal conductivity

Chapter 3

MODEL SETUP AND EXPERIMENTAL SETUP

Simulation of thermal debinding was developed in Ansys Fluent, CFD commercial code. It has capability to adjust standard flow model based on complex physical phenomena during thermal debinding. The novel of the thermal debinding model was user-defined functions. They were custommised in C based programs language. Source term of the continuity equation, Energy Equation, and physical properties were defined. Section 3.1 explained the experiment detail setting up for validation study of the math model. Section 3.2 explained the detail of models for thermal debinding. Then, section 3.3 showed the implementation of thermal debinding model into Ansys Fluent.

3.1 Problem description and experimental setup

A specimen used for thermal debinding was a rectangular bar with the dimension 4.80x3.85x56.8 mm as showed in figure 3.1. It place on stainless steel setter. A furnace heated air with programmable heating profile such as 0.2-0.8 °C/min. Air flows at the velocity of 0.05 m/s.

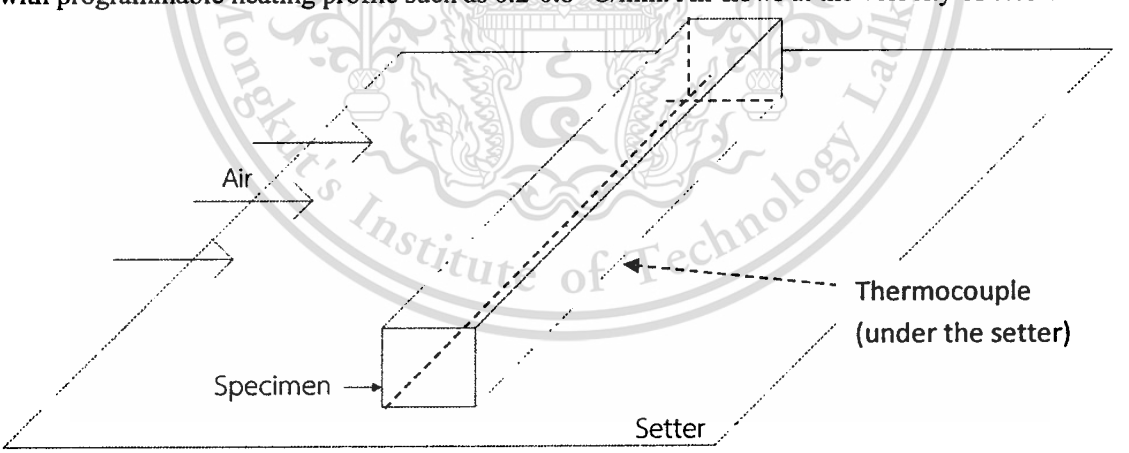

Figure 3.1 Diagram of a specimen on a settle with air flow direction

The stainless steel 316L powder and polypropylene were mixed with 60% and 40% by volume, respectively. A single binder was used in this work because polymer is the main component in the binder system as showed in figure 3.2.

Stainless steel 316L and Polypropylene were mixed together by twin z blade mixing (figure 3.3) machine at 180 °C for 30 minutes. The blend of powder and polymer was called

feedstock. For injection step, the feed stock was injected by Nigata injection machine showed in figure 3.4 into rectangular box shape part, the three point bending specimen, called green part. The parameter setting up for injection machine were velocity of 20 mm/s, pressure of 80 MPa, mould temperature 80 °C. The green parts had measured average weight and average density of 5.250g and 5.100 g/cc, respectively. Green parts had average weight of polypropylene of 0.368 g and average weight of stainless steel powder of 4.882 g. The figure 3.5 showed overall of specimen preparation.

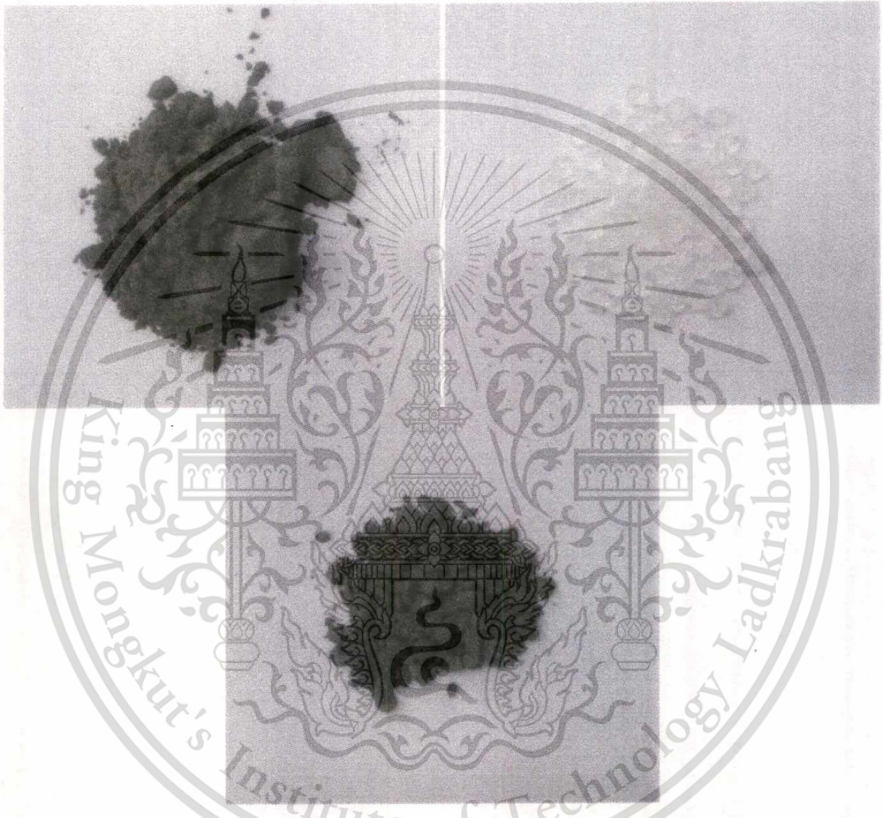

Figure 3.2 Feed stock and raw materials; a) Stainless steel 316L powder, b) polypropylene, and c) feed stock

Experiments of thermal debinding were performed with a few heating rate, 0.2, 0.4, 0.6, 0.8 °C/min. Debinding furnace (showed in figure 3.6) for this work could be supplied by natural air.

For 0.2 °C heating rate of thermal debinding, five specimen were debinded to different temperature such as 160 °C, 200 °C, 250 °C, 300 °C, and 400 °C corresponding with debinding time of 36,000 s, 48,000 s, 63,000 s, 78,000 s, and 108,000 s, respectively. The first specimen was debinded until the temperature reached a target temperature of 160 °C and the specimen was

removed instantly from the furnace for measuring weight. The remaining weight of polypropylene binder in the specimen was calculated by subtracting the different weight after thermal debinding from the weight of polymer which could be written as

$$W = 0.0754W_{green} - (W_{green} - W_{debinded}) \quad \text{..... (3.1)}$$

For other specimen, they were performed in the same manner. However, the target temperatures were changed to 200 °C, 250 °C, 300 °C, and 400 °C. Table 3.1 showed the experiment of debinding with heating profile of 0.2 °C/min. There were 5 specimens were debinding for various of target temperature of 160 °C, 200 °C, 250 °C, 300 °C, and 400 °C, respectively. The experimental procedure of debiding with heating rate of 0.2 °C/min was shown in figure 3.7.

During thermal debinding step, a thermocouple was used to measure the temperature of the setter for define the temperature boundary condition in CFD simulation. The thermocouple was placed under the setter near the centre of the specimen shown in figure 3.1.

Figure 3.3 twin z blade mixing machine

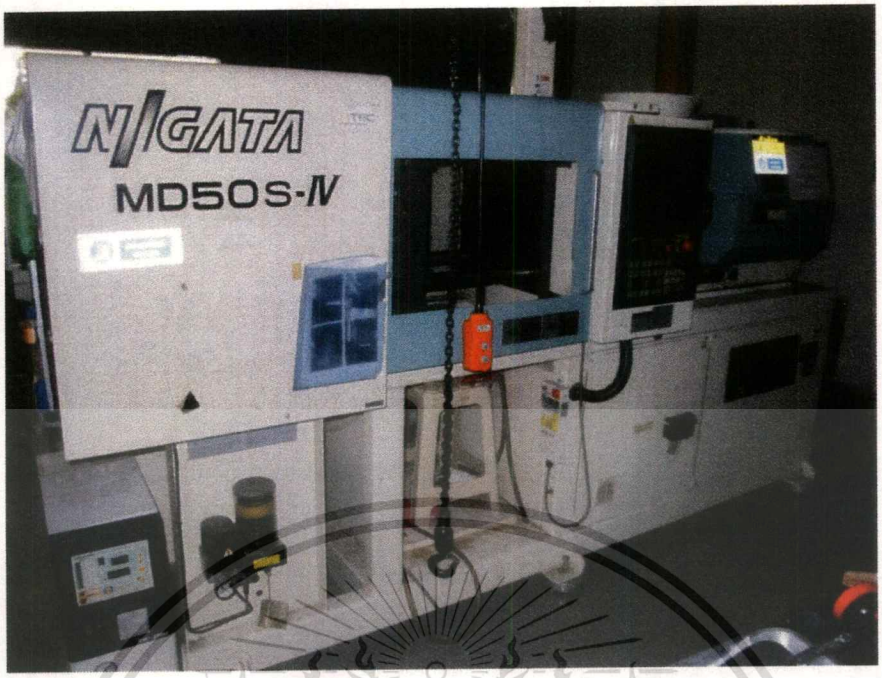

Figure 3.4 Injection machine of Nigata

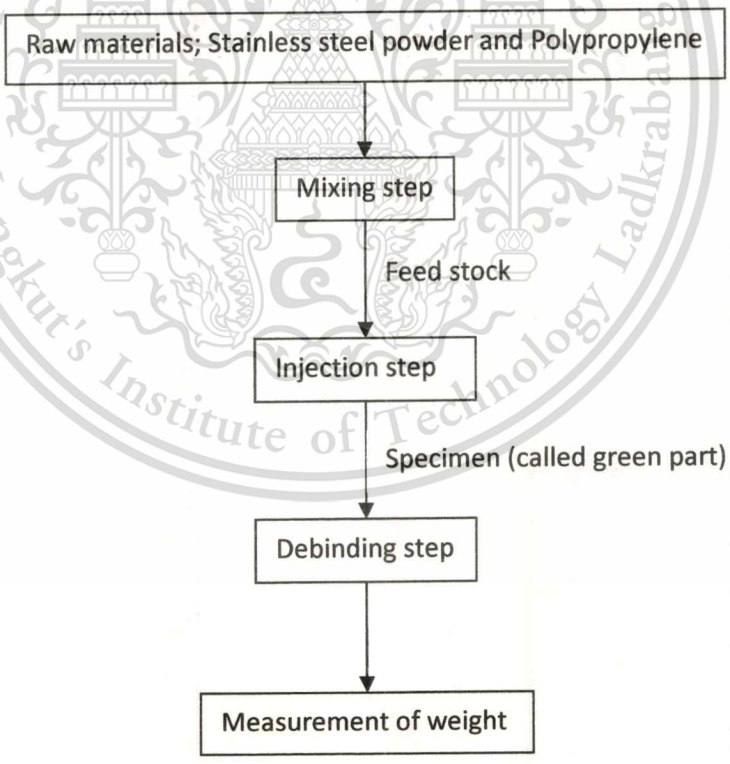

Figure 3.5 Specimen preparation for thermal debinding

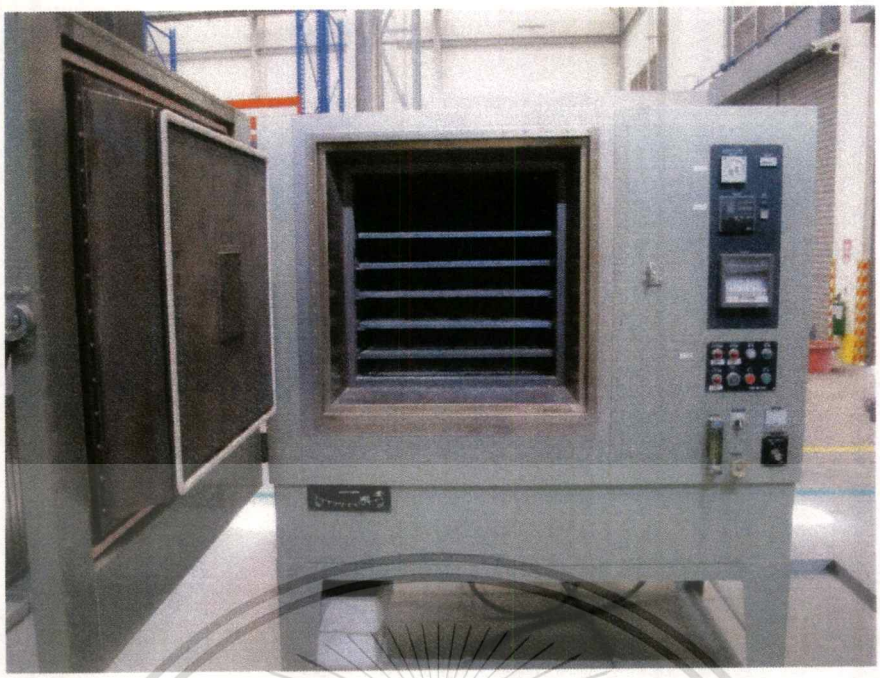

Figure 3.6 Debinding furnace

Table 3.1 Experiment of thermal debinding for heating profile of 0.2 °C/min (single heating reate)

Temperature (°C)	Debinding time (s)	specimen
160	36,000	1
200	48,000	2
250	63,000	3
300	78,000	4
400	108,000	5

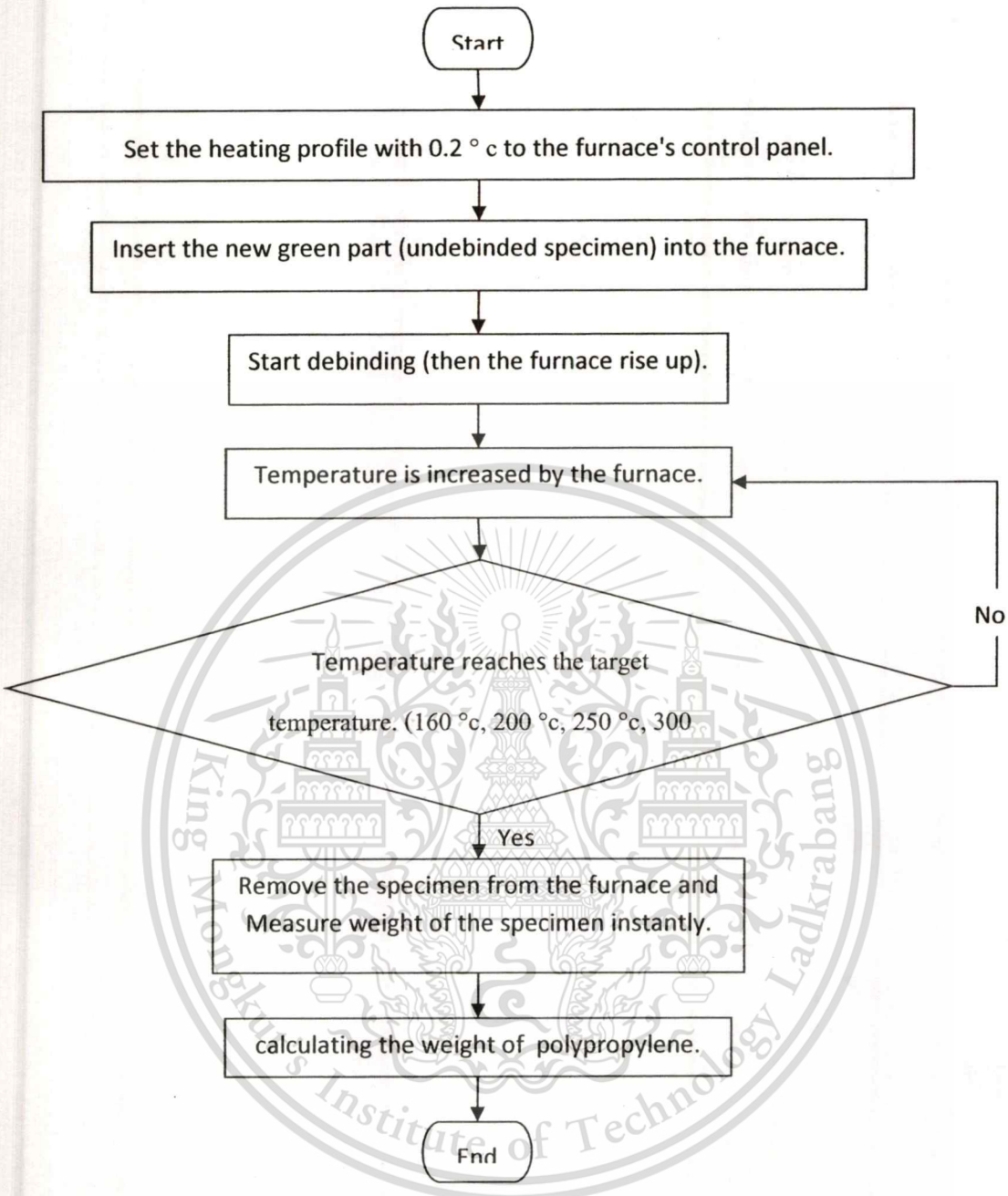

Figure 3.7 Experimental procedure of debiding with heating profile of 0.2 °C/min

For multiple heating rate of 0.2, 0.4, 0.6, and 0.8 °C/min, the debinding were done until temperature reached 200 °C for each specimens as showed in table 3.2. After debinding, all specimen also were measured for the weights to find out remain mass of polymer in the specimen. The experimental procedure of debiding with various heating rates was shown in figure 3.8. Temperature profile used to setup the furnace was shown in figure 3.9

Table 3.2 Experimental of thermal debinding for heating profile of various heating rate

(multiple heating rate)

heating rate °C/min	specimen
0.2	1
0.4	2
0.6	3
0.8	4

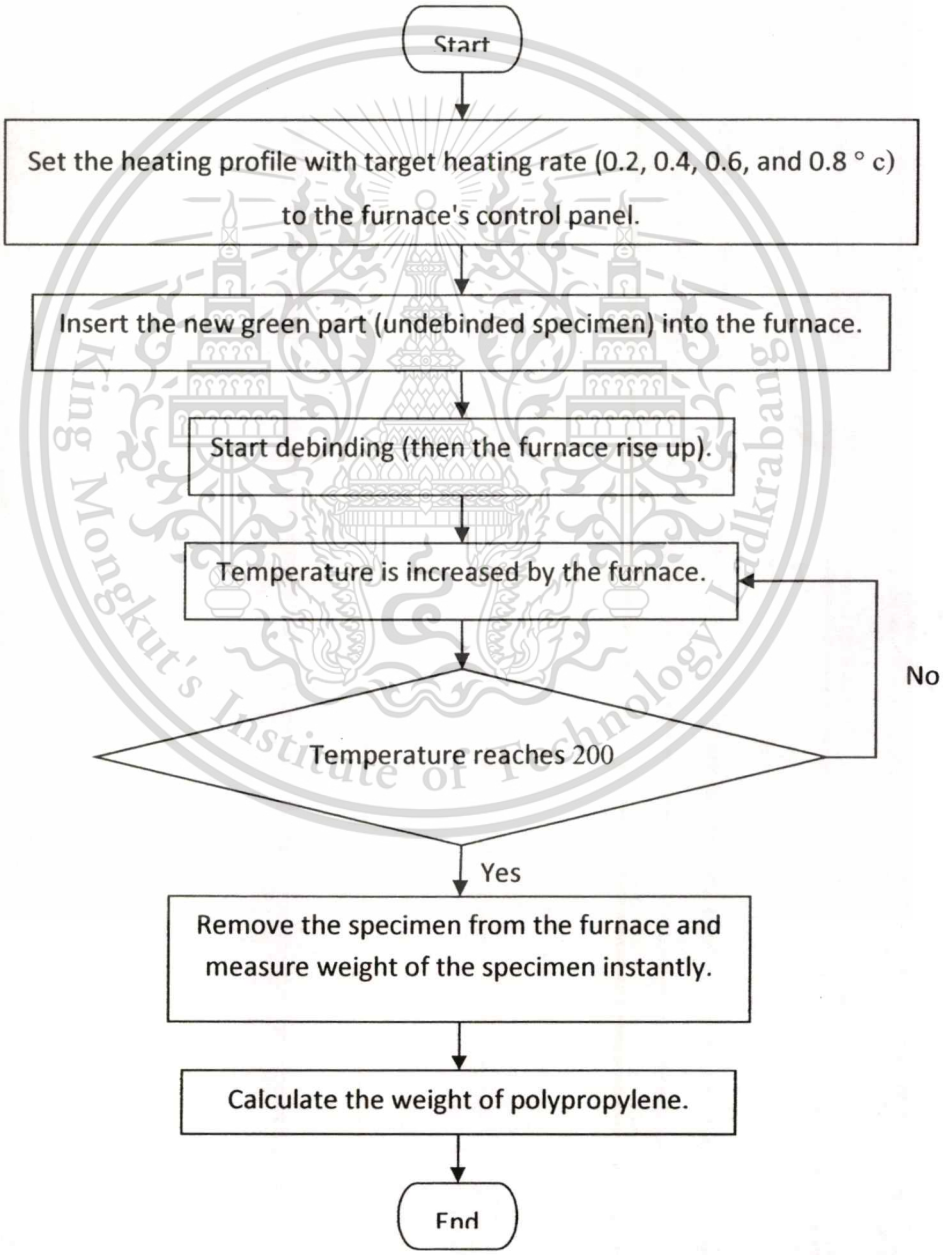

Figure 3.8 Experimental procedure of debiding with heating profile of various heating rate

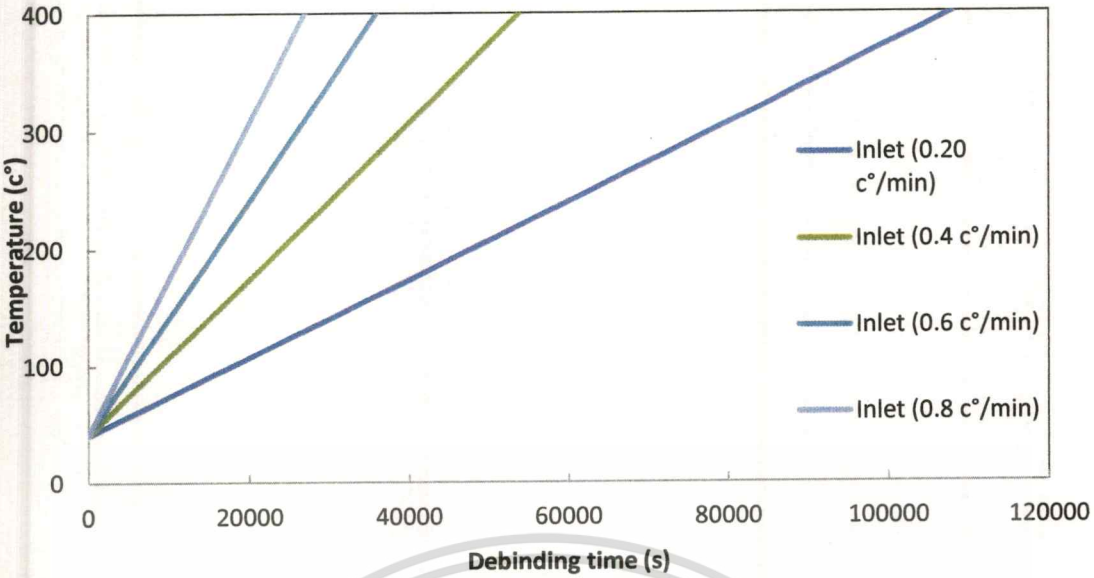

Figure 3.9 Temperature profile used to setup the furnace

3.2 Governing equation for thermal debinding model

Two-dimensional problem is used instead of three dimensional problem because of shorter time in solving numerical model. The cross section at mid-plane of box specimen place inside a furnace is modelled as shown in Fiqure1. There are several assumptions made to simplify the model (Khoong and et al, 2010), which are;

(a) the metallic powder porous media is considered rigid compare with liquid and gas inside specimen.

(b) there is no chemical reaction between metallic powder porous media and gas phase of volatile vapour and air.

(c) the three-phase system of solid powder, liquid polymer and gas inside specimen is considered in local thermodynamic equilibrium.

(d) the total gas phase is considered as a mixture of ideal gases.

(e) the liquid polymer degrades to identical volatile fragment throughout the thermal debinding process.

(g) the liquid phase is assumed to be solid material because the effect of liquid phase flow can be neglected for specimen which is porous material during thermal debinding.

(h) the liquid volatile fragments evaporate into vapour phase almost instantaneously after the thermal degradation of liquid polypropylene polymer.

The model could be used to forecast pressure inside the specimen. However, the melt down and creation of bubble could not be estimated

In the specimen, the governing equations for modelling thermal debinding are modified to capture phenomena of flow in porous media. All governing equations in Euler multiphase model of Ansys Fluent are modelled throughout thermal debinding. The subscripts a and hc stand for air and vapour volatile fragment. All governing equations are described below.

In debinding step, heat transfer to specimen by air flows in furnace. There were a few physical mechanisms to be adopted in the model. The fist is thermal degradation of polypropylene binder. The second is multiphase flow of air and degraded vapor in the furnace environment. The third is gas flow system in porous media.

The governing equation will be simplified to the thermal debinding of single component binder in this chapter. In furnace, the specimen was heated by hot air. Then, the polypropylene binder degraded into vapor of volatile fragment inside the specimen. Then, among of voids increased as vaporisation continued. Consequently, air could diffuse through the porous specimen. Then, The multiphase flow in porous media was considered for thermal debinding.
Continuity Equations for both phases of air ("a" used as subscription) and 1-tetradecene ("hc" used as subscription) are written as:

$$\frac{\partial \alpha \rho_a \phi_a}{\partial t} + \nabla \cdot (\alpha \rho_a \vec{v}_a) = \gamma \sum_{p=1}^{n} \left(\dot{m}_{a,hc} - \dot{m}_{hc,a} \right) + \gamma S_a \quad \text{..... (3.2)}$$

$$\frac{\partial \alpha \rho_{hc} \phi_{hc}}{\partial t} + \nabla \cdot (\alpha \rho_{hc} \vec{v}_{hc}) = \gamma \sum_{p=1}^{n} \left(\dot{m}_{hc,a} - \dot{m}_{a,hc} \right) + \gamma S_{hc} \quad \text{..... (3.3)}$$

Equation 3.1 is the continuity equation of air. There is no the mass transformation between air and 1-tetradecene so term of $\dot{m}_{hc,a} - \dot{m}_{a,hc}$ in equation 3.1 and term of $\dot{m}_{a,hc} - \dot{m}_{hc,a}$ in equation 3.2 can be subtracted and cancelled out. Moreover, there is not a generation of air, S_a also can be subtracted.

Momentum equation system can be written as

$$\frac{\partial(\gamma\alpha_a\rho_a\vec{v}_a)}{\partial t}+\nabla\cdot(\gamma\alpha_a\rho_a\vec{v}_a)=$$
$$-\gamma\alpha_a\nabla p+\nabla\cdot\left(\gamma\overline{\overline{\tau}}_a\right)+\gamma\alpha_a\rho_a\vec{g}+\gamma\sum_{p=1}^{n}\left(\vec{R}_{a,hc}+\dot{m}_{a,hc}\vec{v}_{a,hc}-\dot{m}_{hc,a}\vec{v}_{hc,a}\right)$$
$$+\gamma\left(\sum_{p=1}^{n}\left(\dot{m}_{a,hc}-\dot{m}_{hc,a}\right)\right)+\gamma\left(\vec{F}_a+\vec{F}_{lift,a}+\vec{F}_{vm,a}\right)+\alpha_a\left(\frac{\mu}{K}+\frac{c_{cp}}{2}|\vec{v}_a|\right)\vec{v}_a \quad (3.4)$$

$$\frac{\partial(\gamma\alpha_{hc}\rho_{hc}\vec{v}_{hc})}{\partial t}+\nabla\cdot(\gamma\alpha_{hc}\rho_{hc}\vec{v}_{hc})=$$
$$-\gamma\alpha_{hc}\nabla p+\nabla\cdot\left(\gamma\overline{\overline{\tau}}_{hc}\right)+\gamma\alpha_{hc}\rho_{hc}\vec{g}+\gamma\sum_{p=1}^{n}\left(\vec{R}_{hc,a}+\dot{m}_{hc,a}\vec{v}_{hc,a}-\dot{m}_{hc,a}\vec{v}_{hc,a}\right)$$
$$+\gamma\left(\sum_{p=1}^{n}\left(\dot{m}_{hc,a}-\dot{m}_{a,hc}\right)\right)+\gamma\left(\vec{F}_{hc}+\vec{F}_{lift,hc}+\vec{F}_{vm,hc}\right)+\alpha_{hc}\left(\frac{\mu}{K}+\frac{c_{cp}}{2}|\vec{v}_{hc}|\right)\vec{v}_{hc} \quad (3.5)$$

Some terms in the momentum equation system disappeared. $\vec{F}_{hc}$ and $\vec{F}_a$ can be neglected because there is no other forces in thermal debinding. The lift forces and gravity forces of the both phases are neglected in small system of thermal debinding. For interaction force between phases ($\vec{R}_{pq}$), mass transportation between phases are not considered. Effect of turbulent flow in porous specimen can also be neglected. Then, $C_{2\rho}$ is subtracted. The momentum equations can be written in simplification form as

$$\frac{\partial(\gamma\alpha_a\rho_a\vec{v}_a)}{\partial t}+\nabla\cdot(\gamma\alpha_a\rho_a\vec{v}_a)=-\gamma\alpha_a\nabla p+\nabla\cdot\left(\gamma\overline{\overline{\tau}}_a\right)+\gamma\alpha_a\rho_a\vec{g}+\alpha_a\left(\frac{\mu}{K}\right)\vec{v}_a \quad \text{..... (3.6)}$$

$$\frac{\partial(\gamma\alpha_{hc}\rho_{hc}\vec{v}_{hc})}{\partial t}+\nabla\cdot(\gamma\alpha_{hc}\rho_{hc}\vec{v}_{hc})=-\gamma\alpha_{hc}\nabla p+\nabla\cdot\left(\gamma\overline{\overline{\tau}}_{hc}\right)+\gamma\alpha_{hc}\rho_{hc}\vec{g}+\alpha_{hc}\left(\frac{\mu}{K}\right)\vec{v}_{hc} \quad \text{..... (3.7)}$$

Energy equation system can be written as

$$\frac{\partial(\gamma\alpha_a\rho_a h_a)}{\partial t}+\nabla\cdot(\gamma\alpha_a\rho_a\vec{v}_a\vec{h}_a)=$$
$$\gamma\alpha_a\frac{\partial p_a}{\partial t}+\gamma\overline{\overline{\tau}}_a:\nabla\cdot\vec{v}_a-\nabla\cdot(\gamma\vec{q}_a)+\gamma S_a+\gamma\sum_{p=1}^{n}\left(Q_{a,hc}+\dot{m}_{a,ha}h_{a,hc}-\dot{m}_{hc,a}h_{hc,a}\right)+Q_{sa} \quad (3.8)$$

$$\frac{\partial(\gamma\alpha_a\rho_a h_a)}{\partial t}+\nabla\cdot(\gamma\alpha_a\rho_a\vec{v}_a\vec{h}_a)=$$
$$\gamma\alpha_a\frac{\partial p_a}{\partial t}+\gamma\overline{\overline{\tau}}_a:\nabla\cdot\vec{v}_a-\nabla\cdot(\gamma\vec{q}_a)+\gamma S_a+\gamma\sum_{p=1}^{n}\left(Q_{a,hc}+\dot{m}_{a,ha}h_{a,hc}-\dot{m}_{hc,a}h_{hc,a}\right)+Q_{sa} \quad (3.9)$$

For energy equations, there is no mass transfer between the two phases, $\dot{m}_{a,hc}$ and $\dot{m}_{hc,a}$ can be subtracted. The process of this model is assumed to be in thermal equilibrium so the heat transfer between phases must comply with the local balance conditions. Therefore, $Q_{hc,a}$ and $Q_{a,hc}$ were

zero. Q_{sp} is the heat transfer between solid and fluid which is in equilibrium. The simplification form of energy equations are

$$\frac{\partial(\gamma\alpha_a\rho_a h_a)}{\partial t} + \nabla\cdot(\gamma\alpha_a\rho_a\vec{v}_a h_a) = -\gamma\alpha_a\frac{\partial p_a}{\partial t} + \gamma\bar{\bar{\tau}}_a:\nabla\vec{v}_a - \nabla\cdot(\gamma\vec{q}_a) + \gamma S_a \quad \text{.....(3.10)}$$

$$\frac{\partial(\gamma\alpha_{hc}\rho_{hc}h_{hc})}{\partial t} + \nabla\cdot(\gamma\alpha_{hc}\rho_{hc}\vec{v}_{hc}h_{hc}) = -\gamma\alpha_{hc}\frac{\partial p_{hc}}{\partial t} + \gamma\bar{\bar{\tau}}_{hc}:\nabla\vec{v}_{hc} - \nabla\cdot(\gamma\vec{q}_{hc}) \quad \text{.... (3.11)}$$

Equation 3.3, 3.4, 3.7, 3.8, 3.11, and 3.12 are solved by Ansys Fluent. However, there are a few terms which had to be created and added into the CFD. The commercial software provided normal simple configuration and constant value to general user. Therefore, the simulation of thermal debinding needed special modifications for the Ansys Fluent.

3.3 The user-defined function for thermal debinding model

The degradation of polymer binder gave the reduction of porosity and the initiation of 1-tetradecene vapor. For burn out polypropylene, the energy was consumed in the reaction of degradation. During thermal debinding, the degradation was depended on temperature history of a furnace. Moreover, various heating rate also used in experiments, it was important to consider all as time dependent phenomena. Therefore, 3 main mechanisms were developed into computer codes, C based programming, to modify the default value to the function of time or temperature in Ansys Fluent.

The polypropylene in the specimen was heated during thermal debinding. There was phased transformation such as melting and evaporation which was degradation. The polymer had melted into liquid throughout the specimen before degradation started. An assumption was made that there was not any flow of liquid polymer in the porous specimen. Therefore, the vaporisation was modelled as source term of gas phase of 1-tetradecene. Equation 1.1 was modified based on literature work (Lam Y.C., etal, 2000) was described by

$$S_{hc} = \rho_{l,p}\left(\frac{S_{l,p}}{S_{l,in}}\right)^n A\exp\left(-\frac{E}{RT}\right) \quad \text{..... (3.12)}$$

where $S_{l,p}$ is liquid polymer saturation, $S_{l,in}$ is initial liquid polymer saturation, n is reaction order, A is pre-exponential factor, E is activation energy, and $\rho_{l,p}$ is density of liquid polymer.

The reaction order, pre-exponential factor, and activation energy were obtained from relation of equations in section 2.1 polymer degradation of chapter 2.

Figure 3.10 shows the plots of TGA result. The thermo gravimetric analysis data of polypropylene binder are tested under atmospheric condition. The TGA data of polypropylene is used to calculate the material parameters of the source term in Equation (7). The parameters are obtained by the differential method (Chan and Balke, 1997). The plot of $\ln r - n \ln W$ VS $-\frac{1}{RT}$ was shown in figure 3.11. The activation energy was a slop of. The pre-exponential factor was an intersect. Therefore, the parameters obtained are 87,159.36 kJ/molK for E and 261,569.13 for A

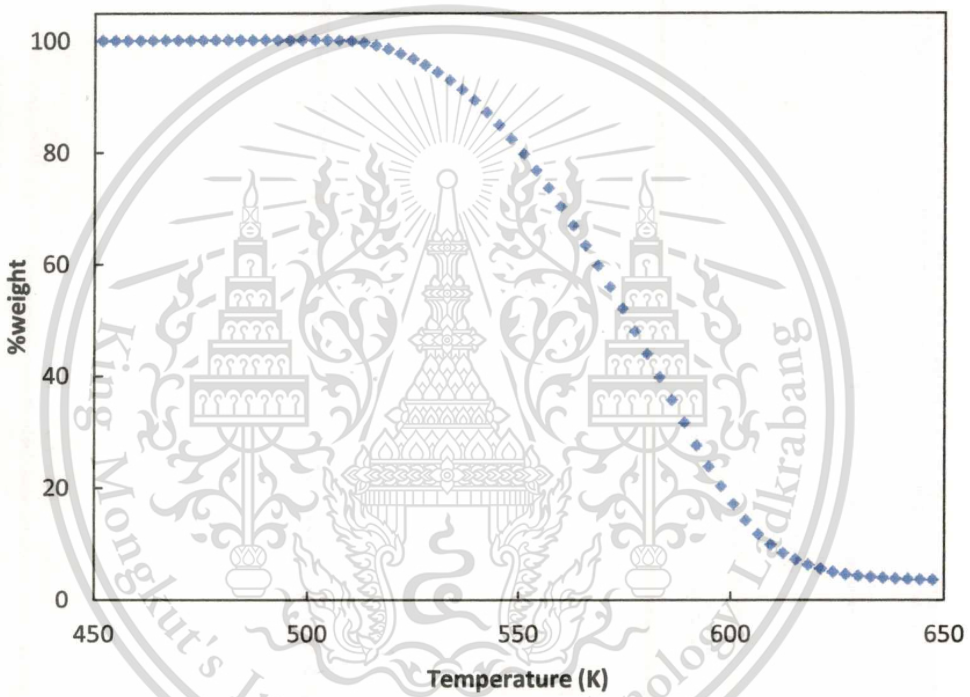

Figure 3.10 Thermogravimetric Analysis results

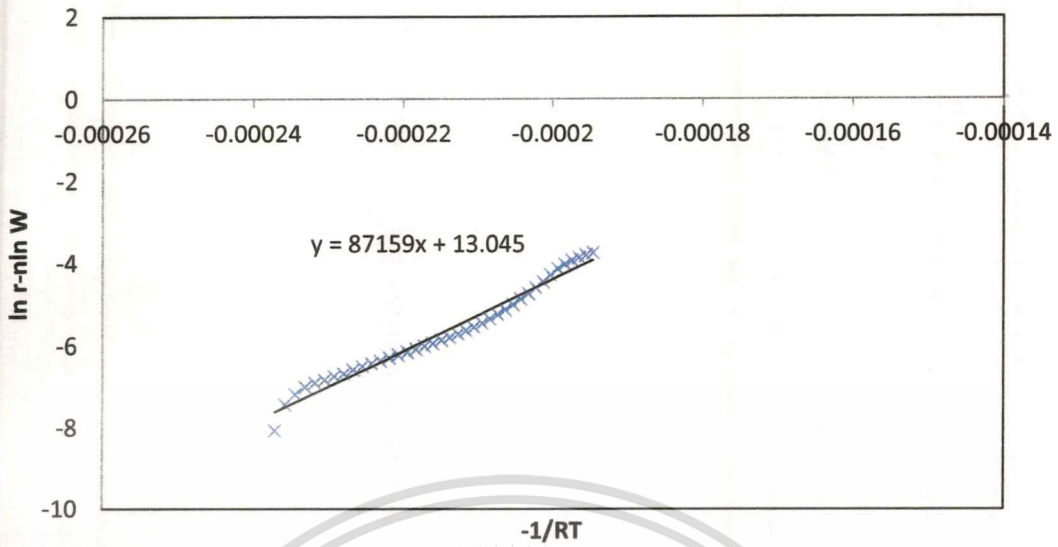

Figure 3.11 least squares to obtain kinetic parameter of thermal degradation

The liquid saturation is the properties of porous media which was a ratio of fluid volume per void volume, written as:

$$S_l = \frac{V_{fluid}}{V_{void}} \quad \text{..... (3.13)}$$

where V_{fluid} is volume of fluid (polypropylene) and V_{void} is volume of void.

The liquid saturation showed fraction of fluid in the void. During thermal debinding, the liquid saturation starts from 1.0 which was initial liquid saturation ($S_{l,in}$). Then, it decreased until the mass polymer was removed out of the specimen.

Porosity decreased during thermal debinding. There were pores after mass of polypropylene had left the specimen. It is a important variable for solving the governing equation system. Moreover, gas phases flow in porous media of thermal debinding needed the porosity. The maximum volume of void was 0.4 time of specimen volume. Therefore, the porosity γ is depended on mass degradation. it is written as:

$$\gamma = \frac{V_{void}}{V_{total}} \quad \text{..... (3.14)}$$

For setting up model, the porosity was needed to define as a function in Ansys fluent. It could be calculated from mass degradation of polypropylene binder. However, the volume of mass loss could be calculated reversely to the volume of void. The total volume V_{total} for Ansys fluent needed to be defined as a volume of cell (or element of mesh).

The crucial point of view flow in porous media is darcy's law which described by eq.11 in chapter 2. The flow in porous specimen is dominated by pressure-driven force because of low velocity. It can be considered as laminar flow. The flow characteristics of gas phase in specimen were depended on viscosity of gas phases. The permeability is defined as

$$K = K_{in}K_r \quad (3.15)$$

where K_{in} is the intrinsic permeability of porous media and K_r is the relative permeability. The intrinsic permeability is the measure of the flow conductance of the metallic powder porous media an d it is estimated as (German, 1981)

$$K_{in} = 4.8 \times 10^{-13} d^{1.3} \varepsilon^{4.8} \quad (3.16)$$

where d is the diameter of metal powder and ε is the porosity of powder without polypropylene. The relative permeability is used to account for the phase distributions. It serves as estimation of the effective permeability of the phases for multiphase flow in a porous media. It is defined in a general empirical correlation as (Udell, 1985)

$$K_r = (1 - S_l)^3 \quad (3.17)$$

Energy sink term was added into Ansys fluent in order to push energy consumption of degradation reaction. The mass degradation of polypropylene was used to calculate the energy sink term by heat of evaporisation which described by

$$S_a = h_{eva} S_{hc} \quad (3.18)$$

where h_{eva} is heat of evaporisation (1-tetradecene)

3.4 Domain of Thermal debinding

The simulation of thermal debinding was conducted thoughtout process which transient problem. A period of time was needed for the simulation. The effective method to reduce simulation time could be archived by transforming model to a two-dimensional problem. The specimen was assumed as a infinite-long rectangular bar.

The specimen was placed on a stainless steel setter inside the furnace shown in figure 3.12. The specimen was a rectangular box. A plan was created such that the section of the specimen became a rectangular shape for 2D problem in figure 3.13.

The domain was simplified to 2D with dimension of 0.0348x0.01985 m. The minimum height of domain was 5 times of height of the specimen. The length of downstream was 7 times of the width of specimen. In fluid region, it was divided into two part that were specimen zone and fluid zone. The specimen zone was a porous media with dimension of 0.00385x0.00480 m which consisted of stainless steel porous and polypropylene binder. The distance from the inlet to the specimen was 0.01000 m. The fluid zone was a region that allowed both air and vapour transport in degraded polymer, 1-tetradecene flow. Air flow from the inlet at x=0.0000 toward x+. During the experiment of thermal debinding, the specimen shown in figure 3.13 was taken out from the furnace to measure the weight.

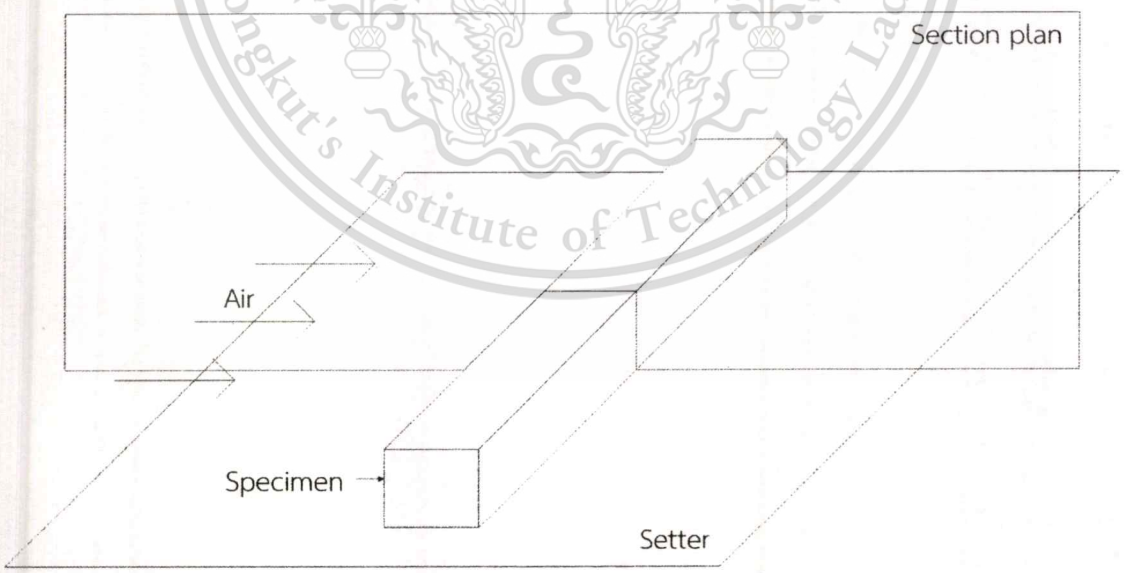

Figure 3.12 Section of specimen and setter for 2D problem

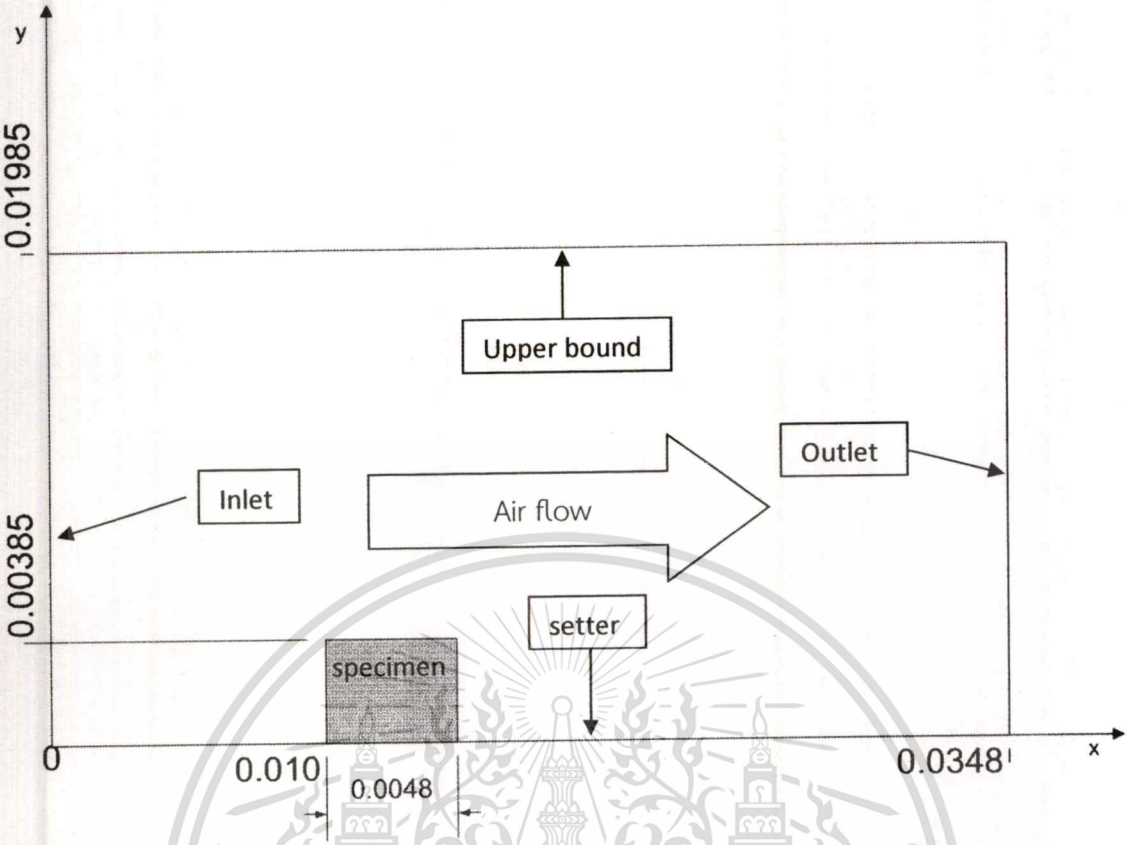

Figure 3.13 Domain of thermal debinding with unit of meters

3.5 Boundary condition

There were 4 types of boundary conditions for the 2D model of thermal deinbing, inlet, upper bound, setter, and outlet. To assign the boundary conditions, air flow in the furnace was assumed to be uniform flow with fan speed of 0.05 m/s shown in figure 3.14. Air could flow across the specimen that could be considered as external flow of air steam. Therefore, the inlet could be applied to be the velocity inlet. The outlet could be assign to be the pressure outlet with as pressure gate equal to 0 because thermal debinding was performed in normal atmosphere pressure. At the upper bound, the wall with slip condition was applied to conform flow could be uniform between inlet and outlet at upper level of air steam. For the setter, wall type of boundary condition was selected with no slip condition because of stationary of the setter.

Thermal debinding was a time dependent process. It takes long time to remove to binder from the specimen. The transient problem could be defined for the model. The temperature also changed with time. The various heating profile were used for this work to investigate weight of specimens under polymer degradation thermally. It was important that the model should be included time-dependent of temperature for boundary condition.

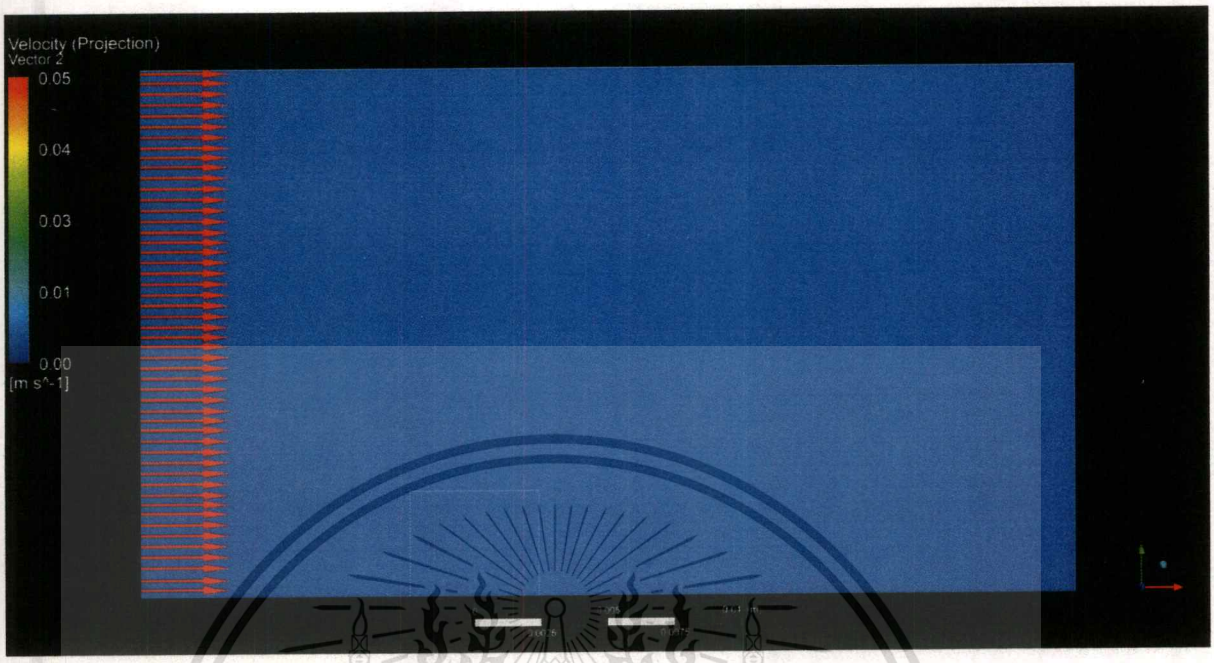

Figure 3.14 Intel velocity profile boundary condition

There were 8 heating profiles used for this work. They could be grouped as 4 couple of heating profiles. The temperature boundary conditions were set to the inlet and the setter that showed in figure 3.15. The model of heating rate 0.2 °C used heating profile of 0.2 °C and 0.19 °C for the inlet and setter, respectively. The other models could be applied the heating profiles in the same way which describing in Table 3.3

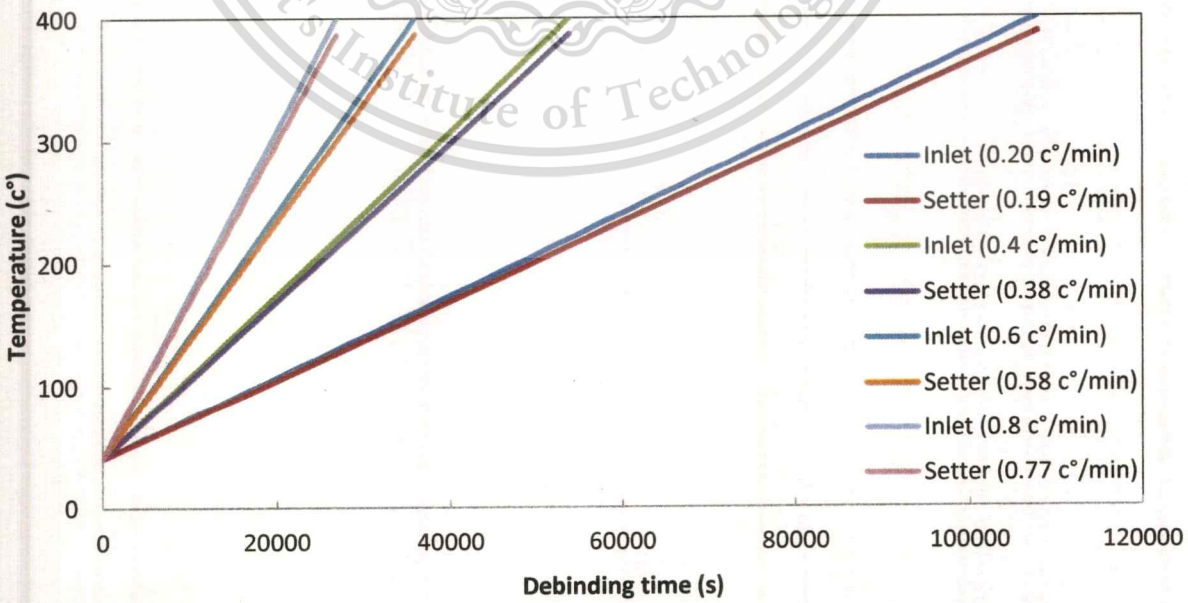

Figure 3.15 Temperature profile of heating rates used for the thermal debinding model

Table 3.3 Couple of heating rates for models of thermal debinding model

	Inlet	Setter
Model of 0.2 °C/min	0.2 °C/min	0.19 °C/min
Model of 0.4 °C/min	0.4 °C/min	0.38 °C/min
Model of 0.6 °C/min	0.6 °C/min	0.58 °C/min
Model of 0.8 °C/min	0.8 °C/min	0.77 °C/min

Temperature of the setter was measured by using thermocouple that was placed under the setter as shown in figure 3.16. The thermocouple was not placed on the specimen to avoid effect of air flow around the specimen. The heated air could dominate the temperature measured on the specimen. Therefore, the thermocouple was placed under the setter in order to reduce the effect of hot air stream. As for the error of temperature measurement was concerned, one could expect that the thermocouple wires were not permitted to contact each other except at the point where measurement was taken. At room temperature, short circuit test was carried out between the thermocouple wires and the test result showed that the thermocouple could perform normally while the wires were in contact to each other (no signal loss was observed).

3.6 Initial condition

All models were started from the temperature of 40 °C or 313.15 K to avoid different ambient temperature between 25 °C to 35 °C. The velocity of x and y component was 0.05 m/s and 0 m/s, respectively. For the volume fraction of 1-tetradecene vapour was 0.0.

3.7 Implementation of user-defined function

Functions called User-defined function developed in section 3.3 could be used in solver. The boundary conditions of thermal debinding were needed to be a function of time. Therefore, they were coded in to Ansys Fluent as a user-defined profile. An used-defined function also be used to monitoring a result of remaining mass. There were nine functions coded into Ansys fluent such as

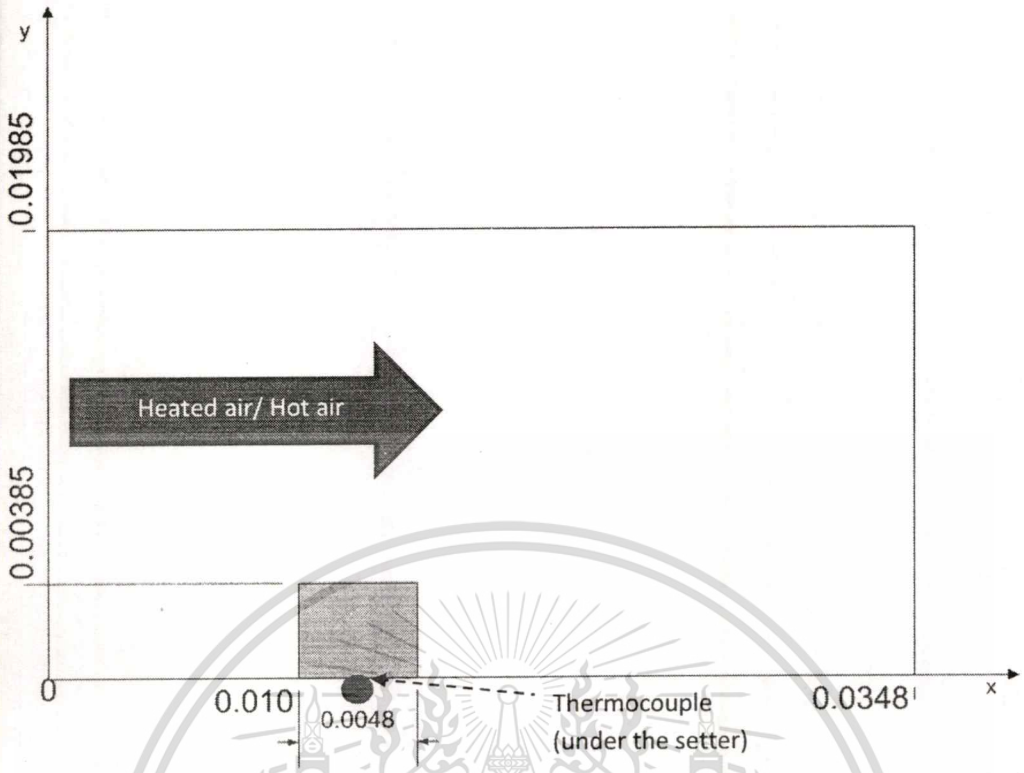

Figure 3.16 Thermocouple place under the setter to measure temperature setter for boundary condition setup

1. Temperature profile of inlet

The temperature profile of inlet was the function control the temperature of Air which entered the domain. Then, the inlet air temperature could be equal to the heating profile that used to setting up the furnace before debinding step. The heating profile for air inlet is defined at the heating rate of 0.2, 0.4, 0.6 and 0.8 °C/min. The temperature profile of inlet could be implemented in the User-defined function in C language as:

```
#include "udf.h"
#include "unsteady.h"
DEFINE_PROFILE(temperature_par,t,i)
{
        #if !RP_HOST
        face_t f;
        begin_f_loop(f,t)
```

```
        {
                F_PROFILE(f,t,i)=273.15+40+0.2*(CURRENT_TIME)/60;
        }
    end_f_loop(f,t)
    #endif
}
```

2. Temperature profile of setter

The temperature profile of settle was applied to settle temperature boundary condition. However, the temperature inside the furnace should be equal for all place, the setter temperature were measured during thermal debindings. The temperature at setter was different with the inlet temperature as approximately 10 °C. Then, the temperature profiles were modified from the inlet temperature profiles to be heating rate of 0.19, 0.38, 0.58 and 0.77 °C/min. The temperature profile of setter could be implemented as

```
#include "udf.h"
#include "unsteady.h"
DEFINE_PROFILE(temperature_wallpart_par,t,i)
{       #if !RP_HOST
        face_t f;
        begin_f_loop(f,t)
                {
                        F_PROFILE(f,t,i)=273.15+40+0.193333333*(CURRENT_TIME)/60;
                }
        end_f_loop(f,t)
        #endif          }
```

3. Porosity

The porosity is defined as the ratio of void of fluid to total volume of void. The specimen was porous solid of stainless steel powder which filled with liquid of polypropylene. The maximum volume of void, equaled to volume of polypropylene mixing in specimen, was 40 percentage. During debinding, the porosity was increases theoretically from 0 to 0.4. The function of porosity could be implemented into Ansys Fluent as

```
#include "udf.h"
```

```
DEFINE_PROFILE(porosity_par,t,i)
{
        #if !RP_HOST
        cell_t c;
        begin_c_loop(c,t)
        {
                if(C_T(c,t)>323.15)
                {
                F_PROFILE(c,t,i)=0.4-(C_UDMI(c,t,2)*0.4);
                C_UDMI(c,t,5)=0.4-(C_UDMI(c,t,2)*0.4);
                }
                else
                {
                F_PROFILE(c,t,i)=0.04;
                C_UDMI(c,t,5)=0.04;
                }
        }
        end_c_loop(c,t)
        #endif
}
```

4. Permeability

The permeability was performed as a function of the intrinsic permeability (K_{in}) and the relative permeability (K_r) which could be coded as

```
#include "udf.h"
DEFINE_PROFILE(gas_vis_res_par,t,i)
{
        #if !RP_HOST
        cell_t c;
        real d=6; /*powder diameter*/
        real epsilon=0.4;
        real k, krg;
```

```
        begin_c_loop(c,t)
        {
                krg=(1-C_UDMI(c,t,2))*(1-C_UDMI(c,t,2))*(1-C_UDMI(c,t,2));
                k=4.8*pow(10,-13)*pow(d,1.3)*pow(epsilon,4.8);
                F_PROFILE(c,t,i)=1/(k*krg);
        }
        end_c_loop(c,t)
        #endif
}
```

5. Mass source

The mass source was a function of polypropylene's kinetic parameters that quantify the degradation of polymer. It estimated the mass generation of 1-tetradecene liquid as defined in equation 3.13. The mass source was a function of density of liquid polypropylene ($\rho_{l,p}$), the liquid saturation ($S_{l,p}$), the initial liquid saturation ($S_{l,in}$), the reaction order (n), the pre-exponential factor (A), and the activation energy (E). The mass source of polymer degradation could be written as

$$S_{hc} = 900\left(\frac{S_{l,p}}{1}\right)^{4} \times 261569.13 \times \exp\left(-\frac{87159.36}{8.314T}\right) \quad (3.19)$$

```
#include "udf.h"
DEFINE_SOURCE(mass_source_par, c, t, dS, eqn)
{       #if !RP_HOST
        real m, T;
        real epsilon=0.4; /*porosity*/
        real rho=900; /*liquid polymer*/
        real Sli=1; /* initial liquid saturation*/
        real r=3.5; /* the reaction order*/
        real c0, Edg; /*constant rate, activation energy*/
        real R=8.314; /* J/mol-k*/
        real sat, temp1,pow_temp1_r,ex;
```

```
if(C_T(c,t)>323.15)
{       if(C_UDMI(c,t,2)>0)
        {       sat=C_UDMI(c,t,2);
                temp1=sat/1.00;
                sat=C_UDMI(c,t,2);
                Edg=87159.36;
                c0=261,569.13;
                pow_temp1_r=pow(temp1,r);
                ex=exp((-Edg)/(R*C_T(c,t)));
                m=epsilon*rho*pow(temp1,r)*c0*ex;       }
}else
{       m=0;    }
C_UDMI(c,t,0)=m;
m=m/C_UDMI(c,t,5);
dS[eqn]=m/C_R(c,t);
return m;       #endif  }
```

6. Heat sink

The heat sink was added to the energy equation of air phase. There was a vaporisation in the specimen. Evaporation needed among of energy for phase change. It could be calculated from equation 3.19. The mass source (S_{hc}) in above section and heat of evaporisation (h_{eva}) was used. It could be written in C language as

```
#include "udf.h"
DEFINE_SOURCE(heat_source_par, c, t, dS, eqn)
{
        #if !RP_HOST
        real m,s;
        real h=238836.134; /*heat of vaporization*/
        m=C_UDMI(c,t,0);
        s=-1*m*h;
        C_UDMI(c,t,3)=s;
        dS[eqn]=0;
```

```
        return s/C_UDMI(c,t,5);
        #endif
}
```

7. Liquid saturation

The liquid saturation was functioned to calculate to fraction of liquid polymer in the void of specimen. Mass of polypropylene in the specimen was used to calculate the liquid saturtion. It could be coded as

```
#include "udf.h"
DEFINE_EXECUTE_AT_END(liquis_saturation_par)
{
        #if !RP_HOST
        Domain *d;
        Thread *t;
        cell_t c;
        real rho=900; /*desity of polypropylene kg/m3*/
        d=Get_Domain(1); /* mixture domain if multiphase */
        t=Lookup_Thread(d,6);
        begin_c_loop(c,t)
        {
                C_UDMI(c,t,2)=0.90-C_UDMI(c,t,1)/(rho*C_VOLUME(c,t)*0.4);
        }
        end_c_loop(c,t)
        #endif
}
```

8. Store mass

The mass source was corrected to the computer memories. During thermal debinding the mass source was accumulated for monitoring history of mass remaining in specimen.

```
#include "udf.h"
DEFINE_EXECUTE_AT_END(store_mass_heat_par)
{
```

```
#if !RP_HOST
Domain *d;
Thread *t;
cell_t c;
real sum=0;
d=Get_Domain(1); /* mixture domain if multiphase */
t=Lookup_Thread(d,6);
begin_c_loop(c,t)
{
        if(C_T(c,t)>323.15)
        {

C_UDMI(c,t,1)=C_UDMI(c,t,1)+C_UDMI(c,t,0)*C_VOLUME(c,t)*CURRENT_TIME
STEP;

C_UDMI(c,t,4)=C_UDMI(c,t,4)+C_UDMI(c,t,3)*C_VOLUME(c,t)*CURRENT_TIME
STEP;
        }
        else
        {
            C_UDMI(c,t,1)=0;
            C_UDMI(c,t,4)=0;
        }
        C_UDMI(c,t,6)=(1-C_UDMI(c,t,1)/0.00606)/C_VOLUME(c,t)*100;
}
end_c_loop(c,t)
#endif
}
```

The functions were used by solver of Ansys Fluent. The boundary condition were assigned to solver before the solving process. Therefore, the user-defined functions of temperature profile of inlet, temperature profile of setter, porosity, and permeability were executed by solver before looping as shown in figure 3.17

After setting up the boundary condition, the source terms of the mass source and the heat sink were called into solver. Then, the governing equation system was solved.

At the end of loop, the function of liquid saturation and stored mass source were executed. These were kept in computer memory. The liquid saturation and stored mass could serve as the values to other function in defining boundary condition next calculation.

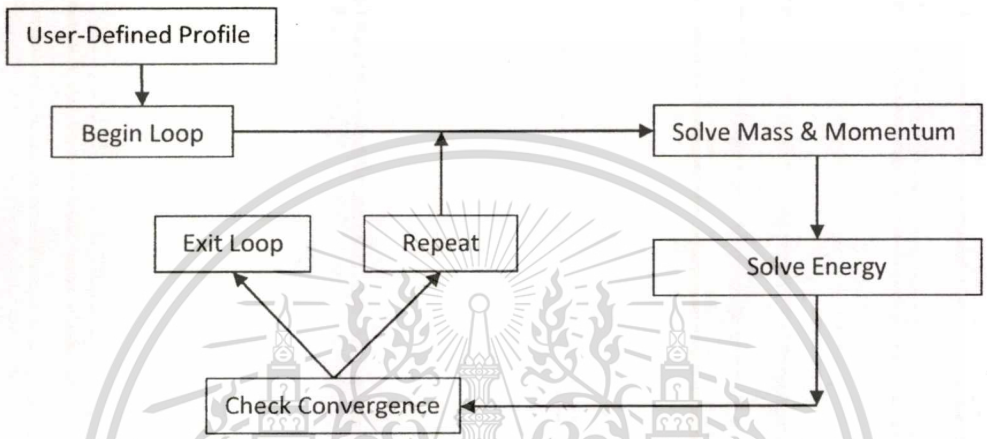

Figure 3.17 Solution procedures for the solver of Ansys Fluent

Chapter 4

MODEL VALIDATION

Validation was done for thermal debinding in various heating rate, 0.2, 0.4, 0.6, and 0.8 c°/min. The heating profile of 0.2 c°/min heating rate was used to debind a specimen. The model predicted mass remained in the specimen by using heating profile of 0.2 c°/min heating rate. There were measurable remaining mass at 200 c° for all heating rate.

4.1 Single heating rate validation

Figure 4.1 shows vapour volatile fragment generation as a function of time. The binder polymer transform into liquid at 360 K corresponding to dibinding time of 14,080 s, which is the temperature for degradation of binder. The mass generation rate of vapour volatile fragment is maximised at 487 K corresponding to 52,240 s which is 1.58×10^{-7} kg/s . This temperature divides the graph into two regions, the *"low temperature"* region and the *"high temperature"* region. The low temperature region is at a temperature range below 487 K. In the low temperature region, the rate of vapour volatile fragment generation increases as the temperature rises. The high temperature region starts is at a temperature range above 487 K. The mass generation in low temperature region takes shorter time period than high temperature region. The mass generation affected the pressure inside the specimen and increased rapidly. There may be bubble created inside the specimen and other deflects such as swelling might occur (Wenjea T.J. and Chung K.H., 1999). Therefore, controlling of thermal debinding at the initial stage in low temperature region is highly critical.

Table 4.1 shows the experiment results of thermal debinding with heating profile of 0.2 c°/min.

There were 4 specimens which were debinded. The first specimen was debinded to the temperature of 160 c°. In the same manner, the other specimens also were debinded to the

temperature as shown in table 4.1. Each specimen was taken out of the furnace instantly when the temperature reached to its designed point for weight measuring. Two replications were performed to ensure minimise affect of experimental error.

Table 4.1 Experimental results of thermal debinding with heating rate of 0.2 c°/min

Temperature (c°)	Debinding time (s)	Residule weight of polymer binder (g)	Percent of binder weight
160	36,000	0.015	96.04
200	48,000	0.094	74.36
250	63,000	0.184	50.06
300	78,000	0.265	28.16
400	108,000	0.358	2.91

Figure 4.2 showed the percentage weight of polymer remaining inside the specimen from numerical model and experimental results. The numerical result shows that the binder polymer degraded from 20,000 s to 100,000 s. There are five experimental weights of polymer that are measured. The first is measured at 36,000 s corresponding to 96% weight remained in specimen. The second was measured at 48,000 s. They were in the low temperature region. The third, fourth, and fifth are measured at 63,000 s, 78,000 s, and 108,000 s, respectively. These three measured weighs are in the high temperature region

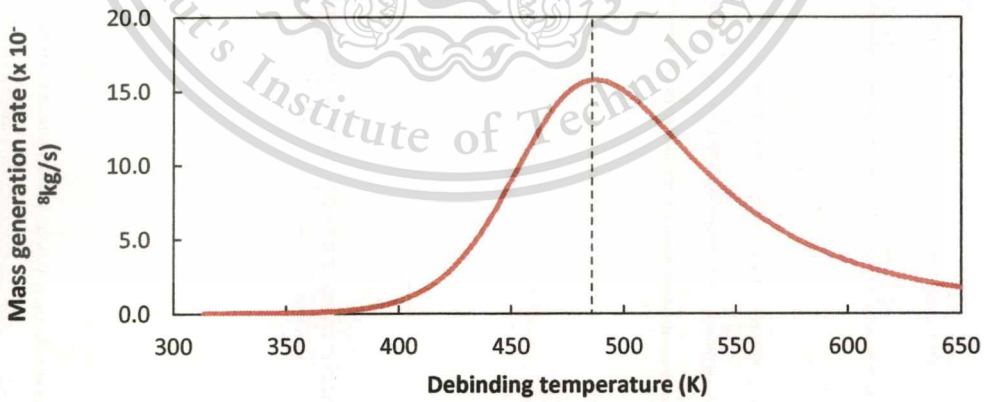

Figure 4.1 Mass generation rate of volatile fragment vapour

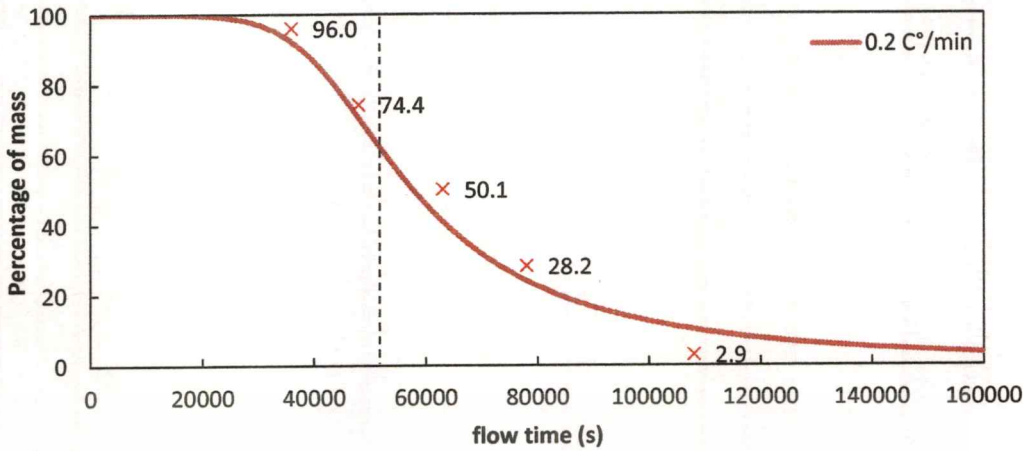

Figure 4.2 Weight of polymeric binder

In the low temperature region, the binder polymer polypropylene melts to liquid and accumulates inside the specimen. The degradation of polypropylene under air ambient is oxidative degradation. The amount of oxygen influents the rate of mass generation of volatile vapour. The mass generation is low at the early stage or the low temperature region, the air can easily react with polymer in the specimen easier. Moreover, the concentration of liquid polypropylene is high. The degradation of polymer is dependent on a concentration of liquid polymer. Therefore, the generation rate of volatile fragment vapour increases until it reaches the maximum rate of 1.58x10e-7 kg/s.

In the second region, binder mass decreases to 61% of total weight. The volatile vapour in the specimen could cause the reaction between oxygen and polymer for the high temperature with less effectiveness than the reaction at low temperature. In addition, the liquid polymer is reduced and caused the mass generation rate of vapour volatile fragment to decrease. The error between the numerical model and experimental results were between 3.8-9.2 percent. The numerical result shows a good agreement with the experiment in the low temperature region. However, more discrepancy is observed during the high temperature region. The model for the thermal debinding is validated and impremented. A damage model can be added to monitor the defection during thermal debinding.

The low temperature region, weight decreased rapidly as suggested by both results of model and experiment. The simulation results of pressure in specimen also increased as showed in figure 4.3. The simulation results predicted the maximum pressure significantly. Polypropylene degraded in the region caused pressure build up inside. The maximum rate of mass loss also occurred in this stage at 52,240s after the maximum pressure point.

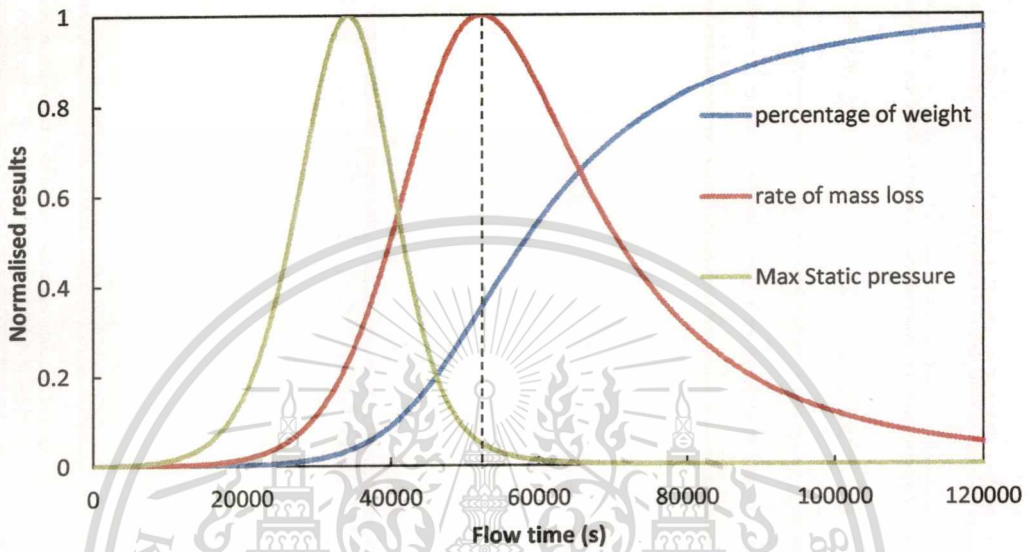

Figure 4.3 Normalised results of thermal debinding model

The maximum static pressure increase to the maximum point at 34,280 s with 2,206.33 Pa was in the low temperature region. The rate of mass loss of polymer binder also increased rapidly from 20,000s to 34,280 s. The mass loss due to degradation reaction was transformed into vapour which was accumulated inside the porous specimen. The generation of gas phase which increased rapidly could caused increment of pressure at the maximum value.

After 34,280 s, the rate of mass loss raised to the maximum point at 52,240. From 34,280 s to 52,240, the rate of mass loss increased with deceleration rate that lead to pressure reduction with lower accumulation of vapour. Therefore, the pressure decreased from maximum pressure point to the ambient pressure. The 35 percentages of polymeric mass also remained in the specimen.

In high temperature region, both pressure maximum in specimen and rate of mass loss decreased. The region was between 52,240 s to the finish of thermal debinding. There was not any pressure build up. It reduce to the normal level early 80,000 s. There was a discrepancy the fifth specimen at 108,000 s. There could be the domination of source term in eq. 3.13 which was recalled as

$$S_{hc} = \rho_{l,p}\left(\frac{S_{l,p}}{S_{l,in}}\right)^{n} A \exp\left(-\frac{E}{RT}\right)$$

The reaction order could give the variation in at the high temperature region. The saturation ration and power of n order in the term of $\left(\frac{S_{l,p}}{S_{l,in}}\right)^{n}$ could lead the mass source (S_{hc}) reduce slowly after debinding time of 91,680 s that saturation ratio was small.

4.2 Multiple heating rate validation

The specimens were debinding with heating profile of 0.2, 0.4, 0.6, and 0.8 c°/min. Each specimens were debinded to the temperature of 200 c°. Then, they were taken out the furnace for weight measurement. The results of all debinded specimens were shown in table 4.2.

Table 4.2 Experimental results of thermal debinding with multiple heating rate

heating rate c°/min	Residule weight of polymer binder (g)	Percent of binder weight (%)
0.2	0.094	74.36
0.4	0.021	94.43
0.6	0.012	96.67
0.8	0.007	98.1

There were 4 heating rates applied to the models to validate that were 0.2, 0.4, 0.6, and 0.8 c°/min with the temperature of 200 c° as showed in figure 4.4. There were good agreements of simulation results with experiment. The experimental percentages of polymer weight remained in the specimen from using heating rates of 0.2, 0.4, 0.6, and 0.8 c°/min were 74.4%, 94.4%, 96.7%, and 98.1%, respectively. The error between results of simulation and experiment were

3.8%, 8.9%, 7.2%, and 6.4% for heating rate of 0.2, 0.4, 0.6, and 0.8 c°/min which were show in table 4.3. The minimum error occurred when the heating rate of 0.2 c°/min was used to simulate. The percentage mass remained at 200 c° decreased with low heating rate was used for both the model and the experiment. There could be variation at the early period of thermal debinding. The degradation reaction continued with accelerated mass loss at the beginning of thermal debinding. The difference between results of the model and experiment could be observed. It was conducted to remind the low temperature region could be the first priority to design the thermal debinding.

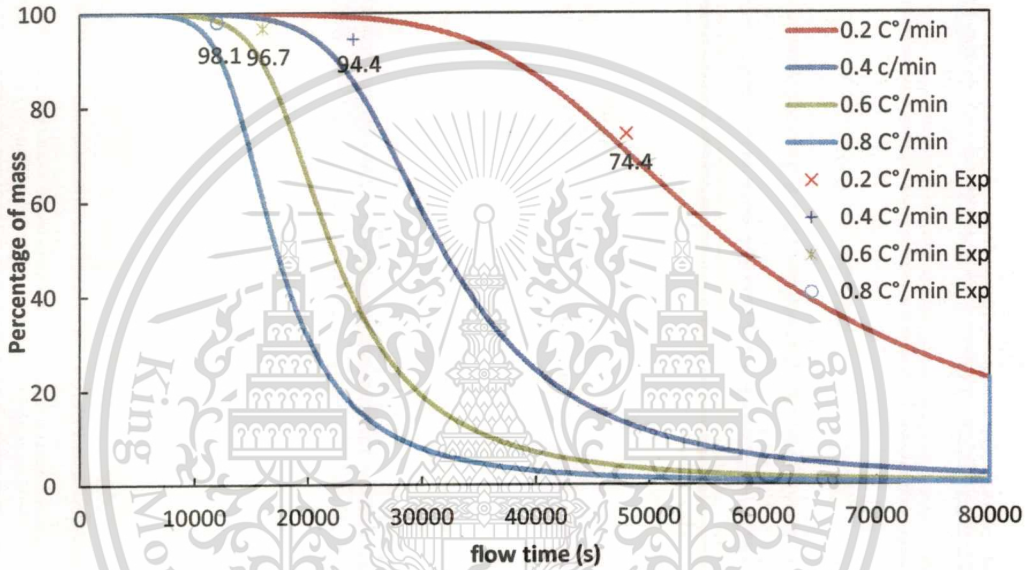

Figure 4.4 validation of thermal debinding model for various heating rate at 200 c°

Table 4.3 The Error of experiments and models were examined at 200 c°.

Heating rate (C°/min)	Error (%)
0.2	3.8
0.4	8.9
0.6	7.2
0.8	6.4

4.3 Parameter sensitivity

Material properties, density, Cp, thermal conductivity, viscosity of Air and 1-tetradecene were studied to estimate sensitivities. Negletable affect could be observed. Due to the uniform temperature distribution of the specimen (as showed in figure 4.6), the degradation could occurred throughout the porous media. For the model using 0.2 c° heating rate, the temperature of specimen was dominated by the setter temperature. The stainless steel setter and the specimen contacted directly. Consequently, the heat could transfer between both specimen and setter greater than between specimen and hot air. The parameter that influence weightloss of specimen thoughtout thermal debinding is the kinetic parameters of polypropylene. Therefore, the reaction order and activation energy were varied which lead to the change of weight of a specimen during thermal debinding as shown in figure 4.7 and 4.8.

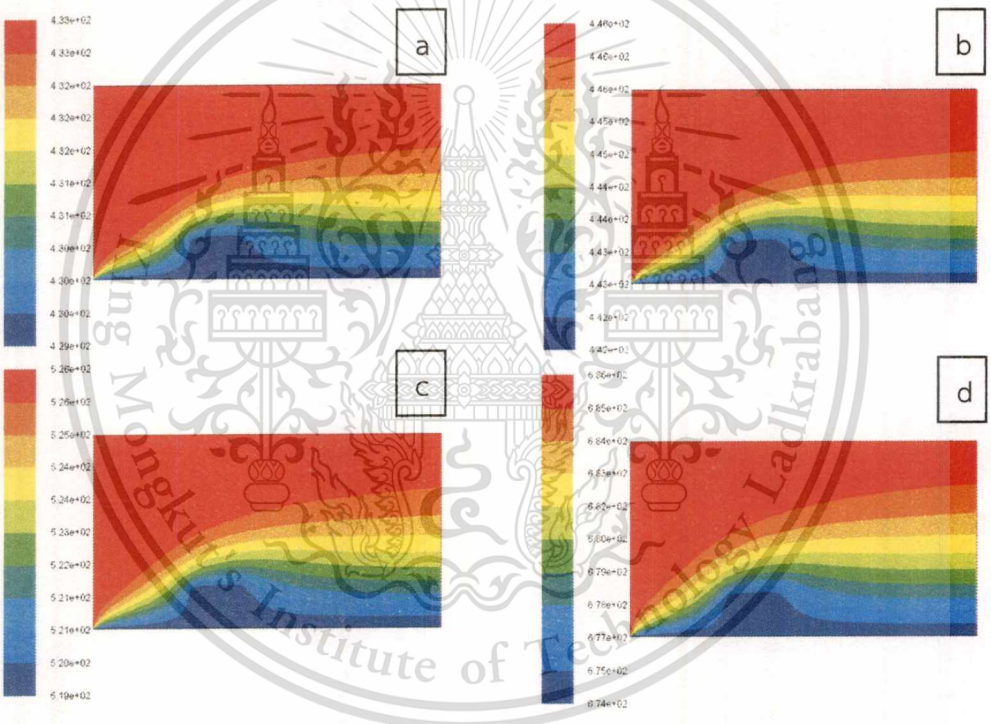

Figure 4.6 temperature distribution of the specimen various debinding time

a) 36,000s, b) 40,000s, c) 64,000s and b) 112,000s

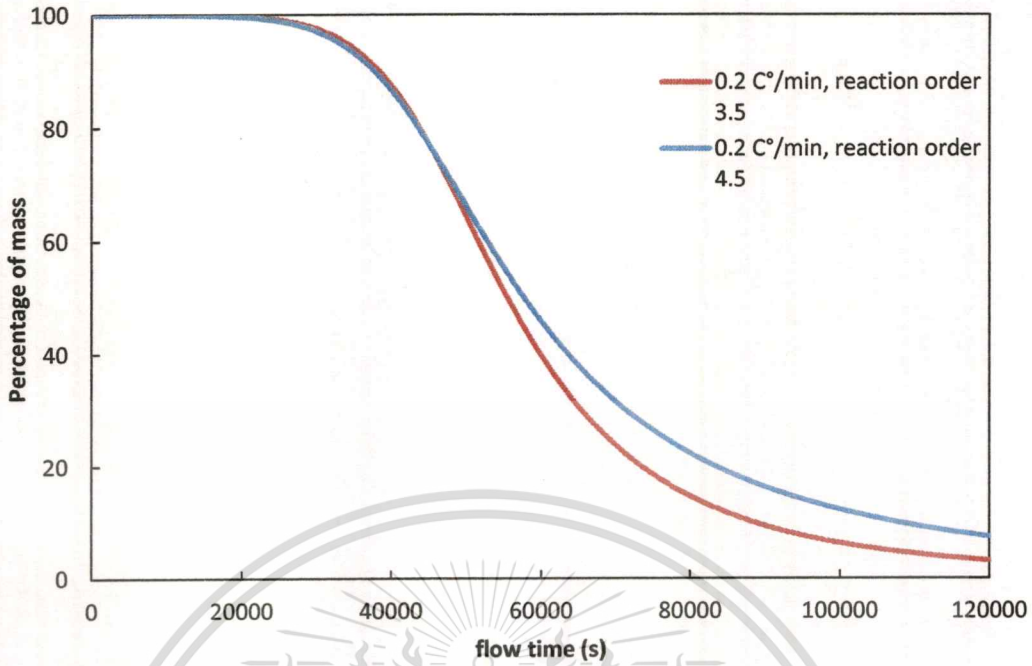

Figure 4.7 Percentages of weight for different reaction order

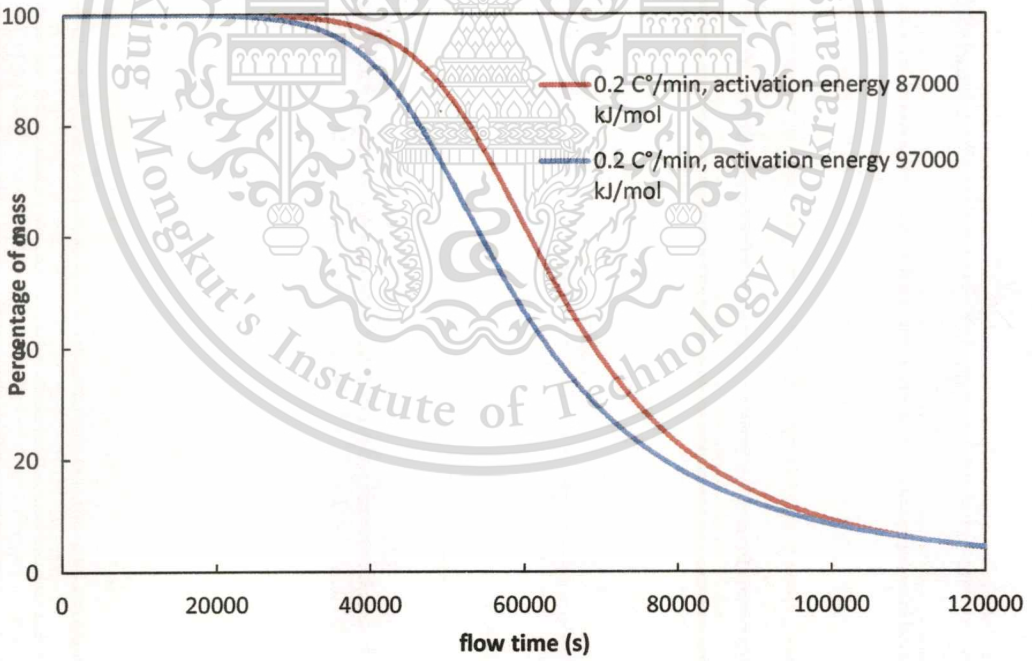

Figure 4.8 Percentages of weight for different activation energy

Chapter 5

PROPOSED HEATING PROFILE FOR DEBINDING A SPECIMEN

The important variable was pressure maximum. The results of multiple heating rate showed that higher heating rate could cause the maximum pressure inside a specimen. The experimental results also indicated the deflect on the specimen. The heating rate of 0.2 °C/min for thermal debinding could be used with no indication of damage. The optimisation was developed based on heating profile of 0.2 °C/min.

5.1 Experimental results

The heating profile of various heating rate such as 0.2, 0.4, 0.6, and 0.8 was used. The specimen wes debinded until the temperature in furnace reached 200 °C. The heating rate 0.2 °C/min for debinding gave an evidence of deflection as showed in figure 5.1 and 5.2.

For heating rates of 0.2, 0.4, 0.6, 0.8 °C/min, there were some indication of damage, deflect, hole, and swelling, on the specimens as shown in figure 5.3. The specimen debinded with heating rate of 0.2 was not perfect. There was a hole at the center of specimen. However, there was no any a hole or deflect on the specimen at section shown in figure 5.3 b which was the specimen debinded with heating rate of 0.4. For debinding with heating rate of 0.6 °C/min and 0.8 °C/min, the specimen could not retain its shape. There could be melting of polymer binder combined with gravity force caused its shape to be distorted. Moreover, the hole inside the specimen could disappear by the gravity effect. The weight of upper part above the center line for specimens using heating rate of 0.6 and 0.8 °C/min could push this portion down as a result the hole was not occurred. This indicates that the specimen was not a rigid body. Therefore, model should not be used for heating rate of 0.6 and 0.8 °C/min as it could not complied with the assumption of the model in chapter 3.

5.2 The simulation results by effect of internal pressure

The model of thermal debinding provided of maximum pressure in the specimen as shown in figure 5.4. The maximum pressure of debinding model with 0.8 °C/min was at 10,800s. However, the lower heating rate of 0.6, 0.4, and 0.2 °C/min was at 13,840s, 19,380s, and 34,360s. The higher heating rate caused the temperature of specimen reached degradation temperature of polymer binder rapidly as mentioned in section 4.2.

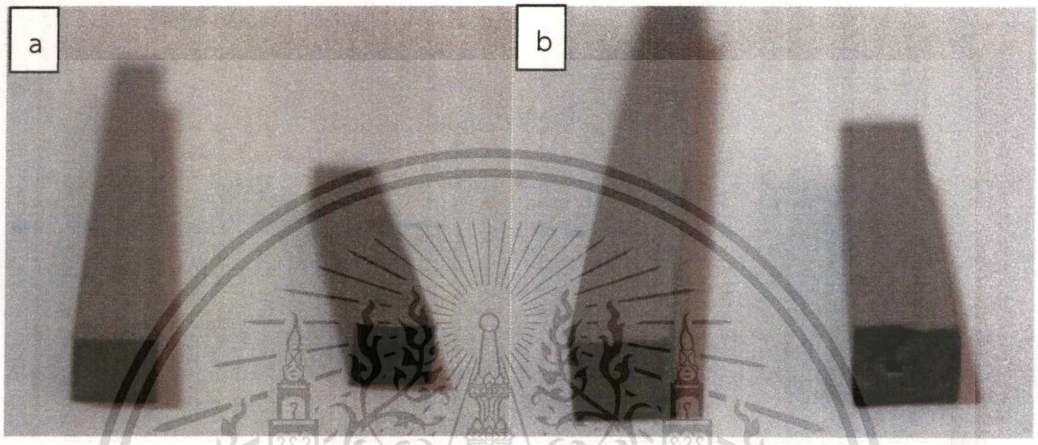

Figure 5.1 specimen debinded to various temperature using heating rate of 0.2 °C a) debineded to 160 °C and b) debined to 200 °C

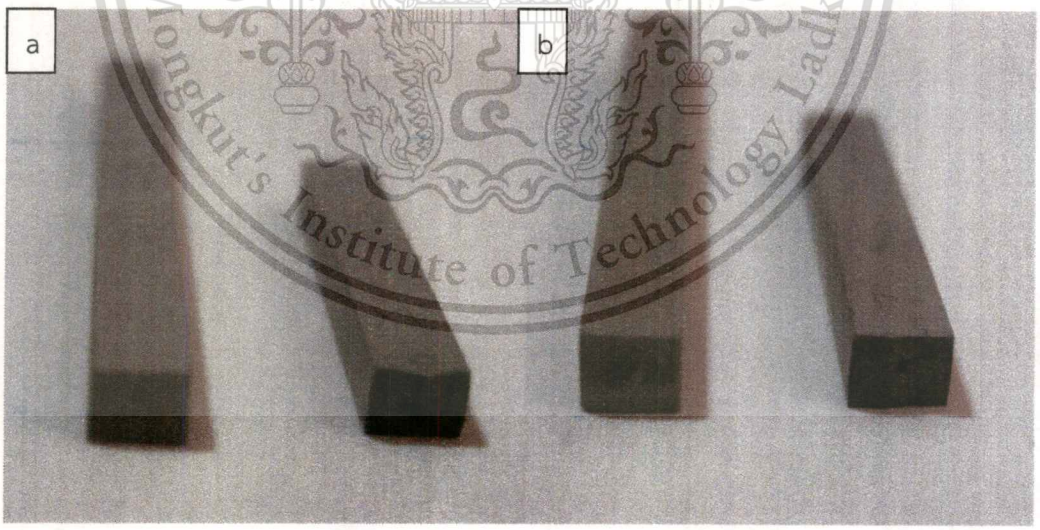

Figure 5.2 specimen debinded to various temperature using heating rate of 0.2 °C a) debineded to 220 °C and b) debined to 250 °C

The pressure build up in the specimens could be different at various heating rate. Using heating rate of 0.8 °C/min, the highest maximum pressure occurred was 8,462.93 Pa. The lower maximum pressure was 6,361.64, 4261.76, and 2206.05 Pa which was from using heating rate of 0.6, 0.4, and 0.2 °C/min, respectively. The pressure in the specimen could be depended on the mass generation of degraded polypropylene. For higher heating rate such as 0.8 °C/min, the specimen was heated up to degraded temperature. Then, the mass generation continued rapidly as the temperature increased.

In order to describe pressure build up, the temperature had to be illustrated to conduct the heat and mass transfer relation. Figure 5.5 showed temperature of air around the specimen. Hot air, flowing across the specimen with higher temperature, caused heat transfer to the specimen. The specimen had temperature of 429 °C equally throughout the specimen. Therefore, the mass generation rate was the same in the specimen region.

The pressure in specimen of debinding model with heating rate of 0.2 °C/min was shown in figure 5.6. The pressure was highest of 2,120 Pa in the centre of specimen. At the outer surface of specimen, the pressure equaled to surround gas. At outer area, the mass near the surface could transform more conventionally than that from the inner region. Because of the same rate of mass generation, there mass accumulation in specimen which could increase the pressure. Moreover, there could be bubble created in the centre region due to gas phase generation. The maximum pressure that occurred at centre of the specimen from simulation results could effect to the gas bubble formation in the specimen. The internal pressure exceeding atmospheric pressure could conducted to create the hole inside the specimen (West and Lombardo, 1998). The internal pressure were studied in several research (West and Lombardo, 1998 and Sachanandani and Lombardo, 2011) which found that they higher than atmospheric pressure between 0-19,000 Pa. However, the internal pressure was depended on specimen dimension, heating rate, polymeric binder.

The results of pressure at 200 °C of all heating profile were showed in figure 5.4. The heating profiles with heating rate 0.2, 0.4, 0.6, and 0.8 °C/min gave internal pressure at 200 °C of 192.12, 1,004.72, 2,506.27, and 4,579.47 Pa. respectively. The monitored pressure at 200 °C was lower than pressure maximum for all heating rate. The experimental results supported the simulation results as the hole inside the specimens was observed when the temperature reached

200 °C. During thermal debinding, temperature increased. It could conduce to gas generation then pressure also increased. As a result, a hole or swelling could occur.

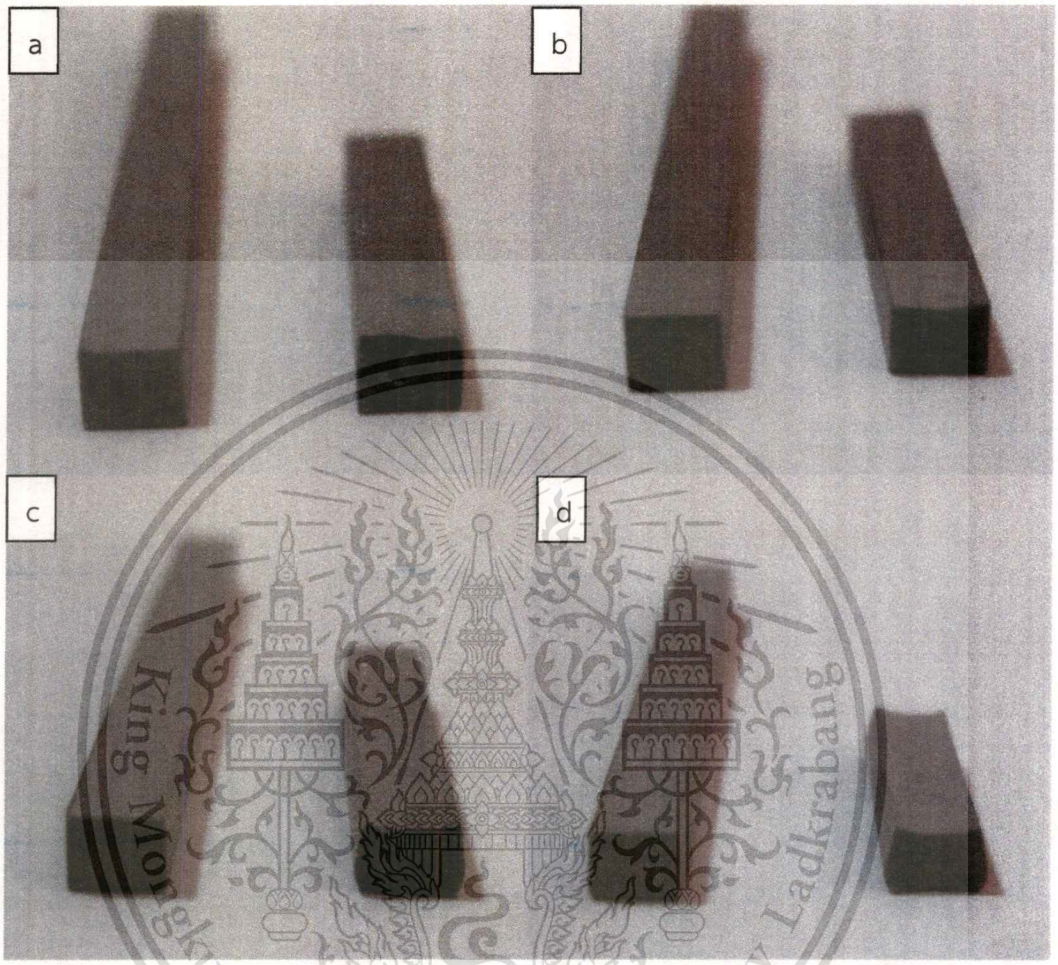

Figure 5.3 Specimen debinding from various heating rate at 200 °C
a) 0.2 °C, b) 0.4 °C, c) 0.6 °C, and d) 0.8 °C

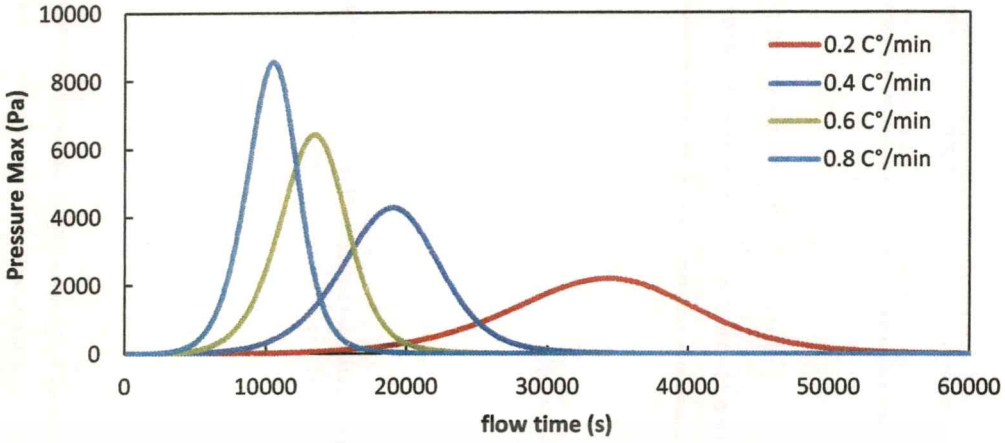

Figure 5.4 Maximum pressure of various thermal debinding models

Figure 5.5 Temperature distribution of the model of 0.2 heating rate at 36,000s

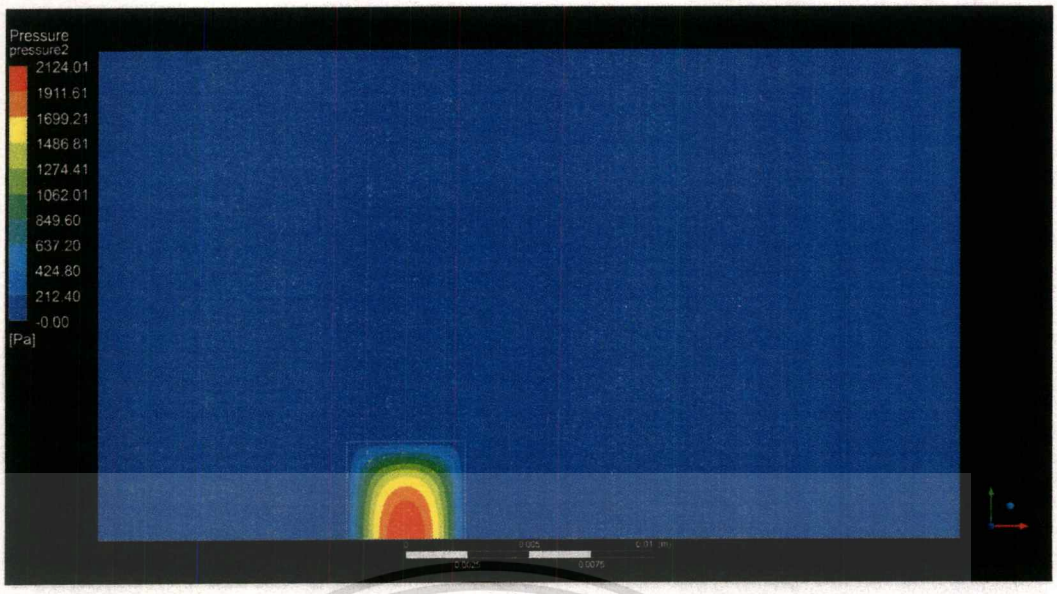

Figure 5.6 Contour of pressure of the thermal debinding model with 0.2 °C/min at 36,000 s.

Internal pressure of all specimens from various heating rates was shown in figure 5.7-5.10. All pressure contours was at 12,000 s. of debidning time. The internal pressures were highest at the center of all lower edges. However, magnitude was difference for all specimens because each highest pressure occurred at different debinding time as shown in figure 5.4

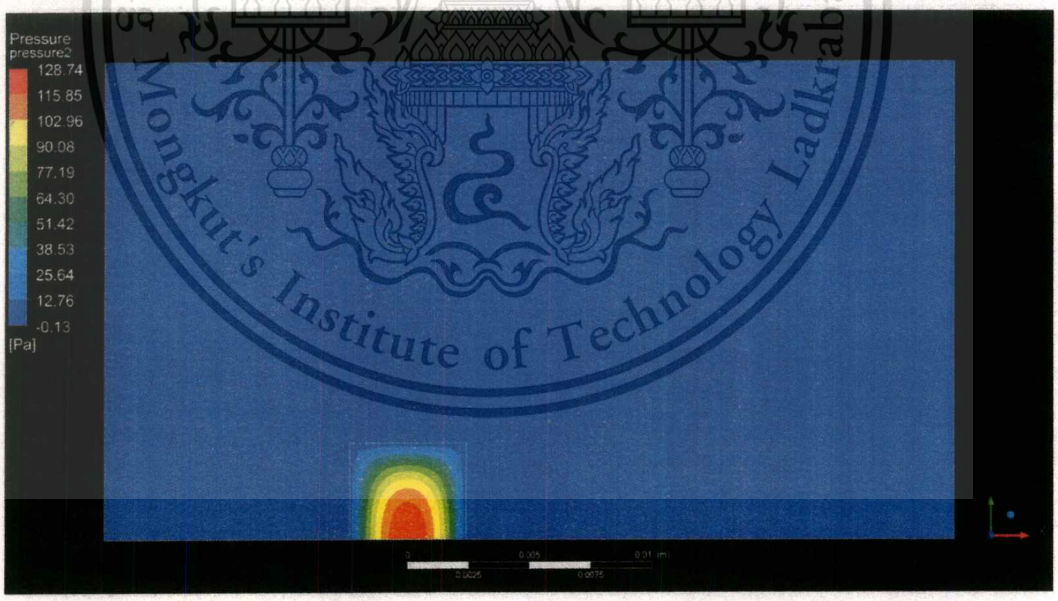

Figure 5.7 internal pressure of the specimen debinded with 0.2 °C/min at 16,000 s of debinding times

Figure 5.8 Internal pressure of the specimen debinded with 0.4 °C/min at 16,000 s of debinding times

Figure 5.9 Internal pressure of the specimen debinded with 0.6 °C/min at 16,000 s of debinding times

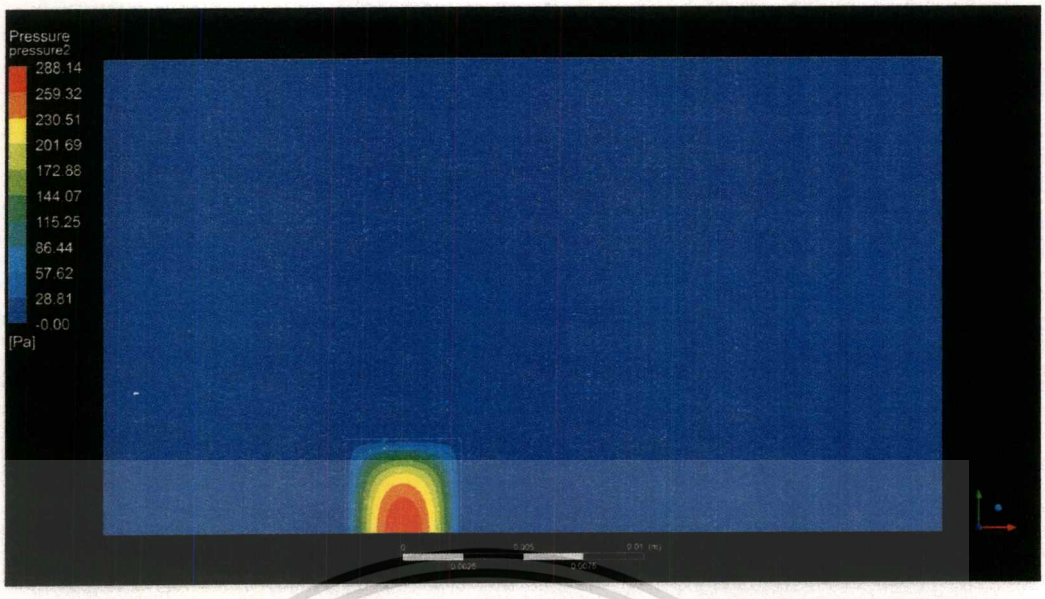

Figure 5.10 internal pressure of the specimen debinded with 0.8 °C/min at 16,000 s of debinding times

5.3 Heat and mass transfer in the specimen

Heat transferred into the specimen from several routes. The conduction and convection could be dominated to the temperature distribution. The heat could transfer from the hot air into the specimen by convection and conduction. However, the setter was the stainless steel which was the same materials with the specimen, heat transfer between the setter and the specimen should be better than between the hot air and the specimen. At initial state of thermal debiding, the specimen consists of stainless steel powder and polypropylene binder. Therefore, the thermal conductivity of the specimen is

$$k_{specimen} = 0.6k_{ss316L} + 0.4k_{pp} \quad \text{.....(5.1)}$$

where thermal conductivity of stainless steel (k_{ss316L}) is 18.0 W/mK and Thermal conductivity of polypropylene (k_{pp}) is 0.2 W/mK. The thermal conductivity of the specimen is depended on volume faction of both stainless powder (0.6) and polypropylene (0.4). Then, the thermal conductivity is 10.88 W/mK. At the final state of thermal debinding, the polymer binder is removed from the specimen. As a result, the thermal conductivity of the specimen equals thermal conductivity of stainless steel which written as

$$k_{specimen} = 0.6k_{ss316L} + 0 \times k_{pp} \quad \text{.....(5.2)}$$

The thermal conductivity of the specimen is 10.80 W/mK. Therefore, the temperature of the specimen was dominated by setter temperature.

The simulation results showed the temperature distribution of the specimen uniformly. The temperature differences (for any given time) over the specimen are small as shown in figure 5.11-5.14. The maximum temperature difference is approximately 0.2. As a result, the liquid polymer begins to degrade throughout the whole compact almost simultaneously.

The degradation was depended on the temperature of the polymer inside specimen. However, the temperature distribution of the specimen was uniform equally in all region of the specimen. The degradation also occurred with the same magnitude. The volatile vapour could flow out easily at the two side surface and the upper surface. The gas phases could not flow out the specimen at the bottom surface because of the perfect contact between the specimen and the setter which was a wall. The volatile vapour at the centre area accumulated because volatile flowed out was not balance with the generation of volatile. In addition, flow of gas inside the specimen was depended on the porosity which the flow was obstructed by porous medium. As a result, the pressure was buildup in the specimen.

Figure 5.11 Temperature distribution of the specimen at 36,000 s. debinded with heating rate of 0.2 °C/min

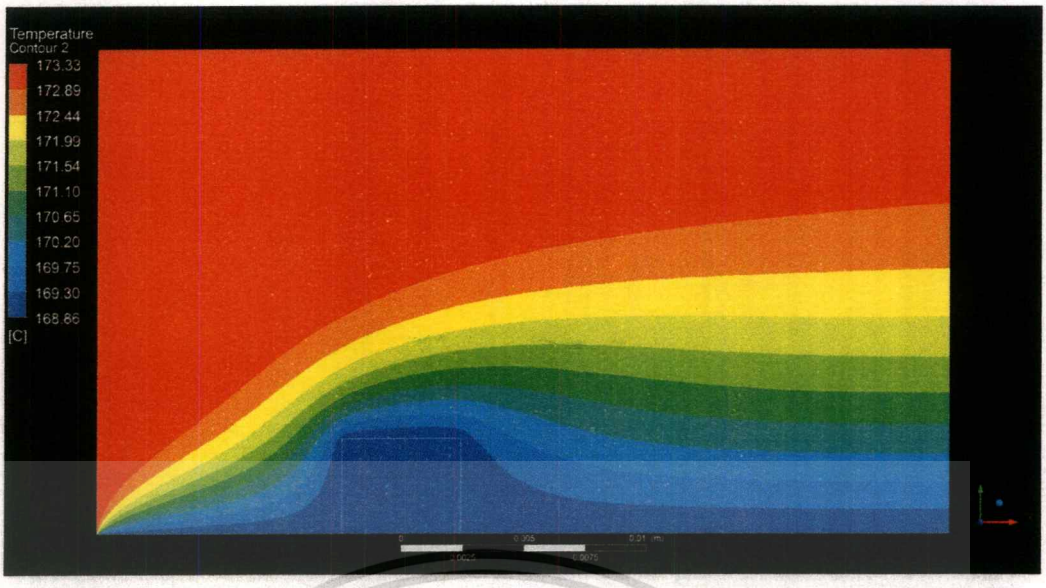

Figure 5.12 Temperature distribution of the specimen at 40,000 s. debinded with heating rate of 0.2 °C/min

Figure 5.13 Temperature distribution of the specimen at 64,000 s. debinded with heating rate of 0.2 °C/min

Figure 5.14 Temperature distribution of the specimen at 112,000 s. debinded with heating rate of 0.2 °C/min

Velocity vector of gas flow inside the specimen at various debinding times showed in figure 5.15-5.18. At the upper surface of the specimen, the velocity of gas flow out was higher than at two upper corners. The direction of gas flow out was quite perpendicular near the centre of the upper surface of the specimen. At the two side surface of the specimen, the velocity of gas flow was highest at the lower corners. The lower velocity of the side surfaces was also at the two upper corners of the specimen.

Figure 5.15 Vector of velocity inside the specimen at 12,000 s. debinded with heating rate of 0.2 °C/min

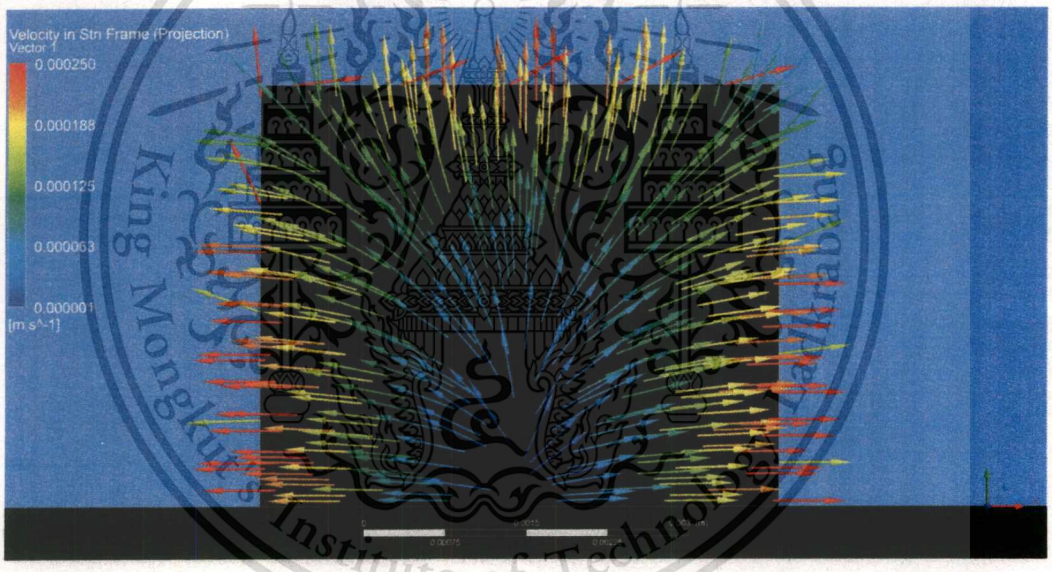

Figure 5.16 Vector of velocity inside the specimen at 36,000 s. debinded with heating rate of 0.2 °C/min

Figure 5.17 Vector of velocity inside the specimen at 64,000 s. debinded with heating rate of 0.2 °C/min

Figure 5.18 Vector of velocity inside the specimen at 112,000 s. debinded with heating rate of 0.2 °C/min

Vector velocities of gas phase flow with heating rate of 0.2, 0.4, 0.6 and 0.8 °C/min in the specimen were plotted in figure 5.19-5.22, respectively. The velocity profile could be considered as the similar profile of all heating rates. The mass flow of gas phases in the specimen was outward and perpendicular to the outer surfaces. At the all upper corners the vector were not perpendicular because of the resultant of combining velocity from the two surfaces the corners.

Differences of velocity magnitudes were observed that because the gas phases were generated maximally with different debinding time as shown in figure 5.4. As a result, the pressure buildup effected to the velocity magnitude differently.

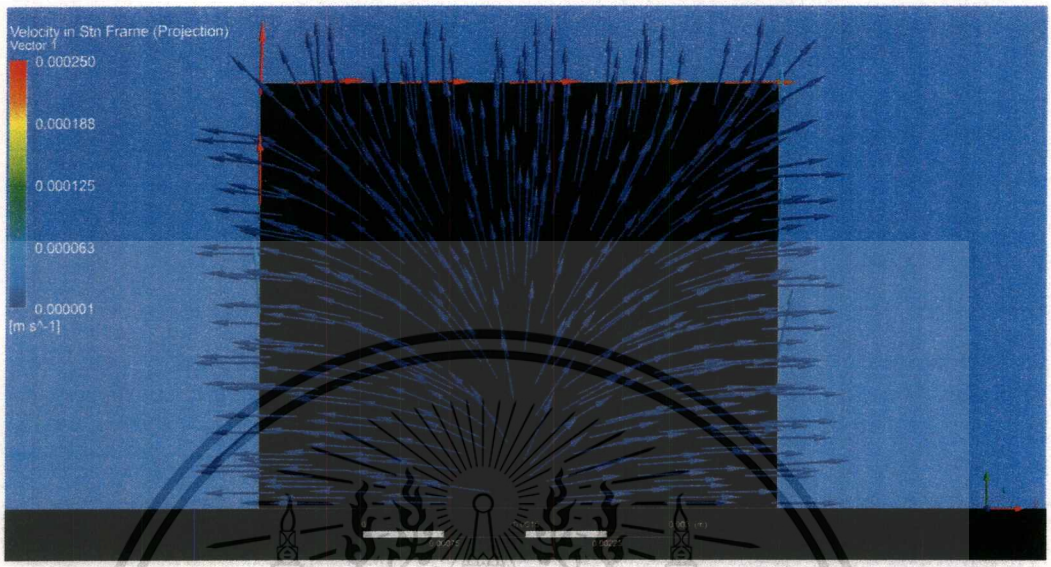

Figure 5.19 Vector of velocity inside the specimen at 16,000 s debinded with heating rate of 0.2 °C/min

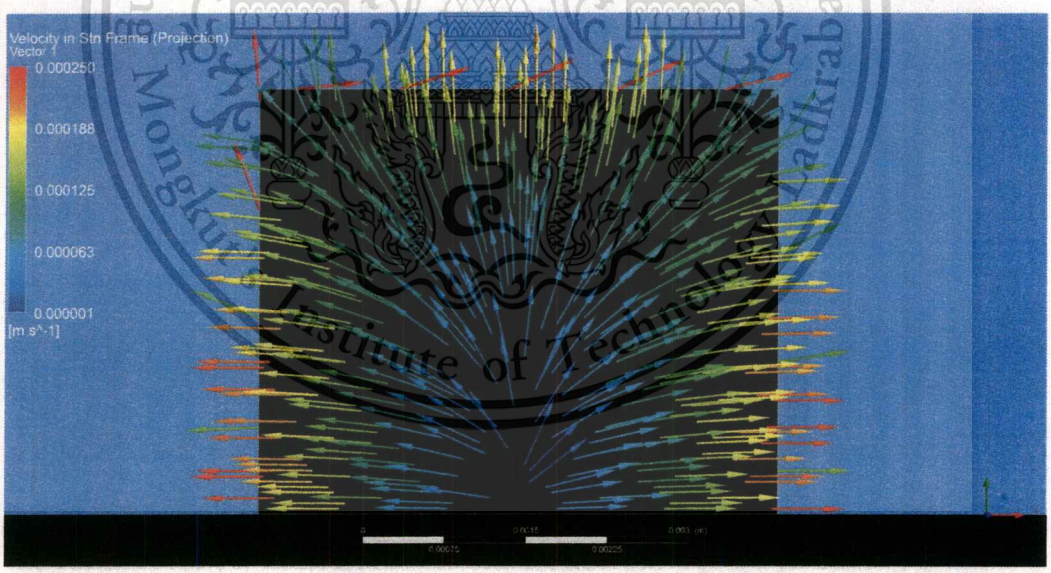

Figure 5.20 Vector of velocity inside the specimen at 16,000 s debinded with heating rate of 0.4 °C/min

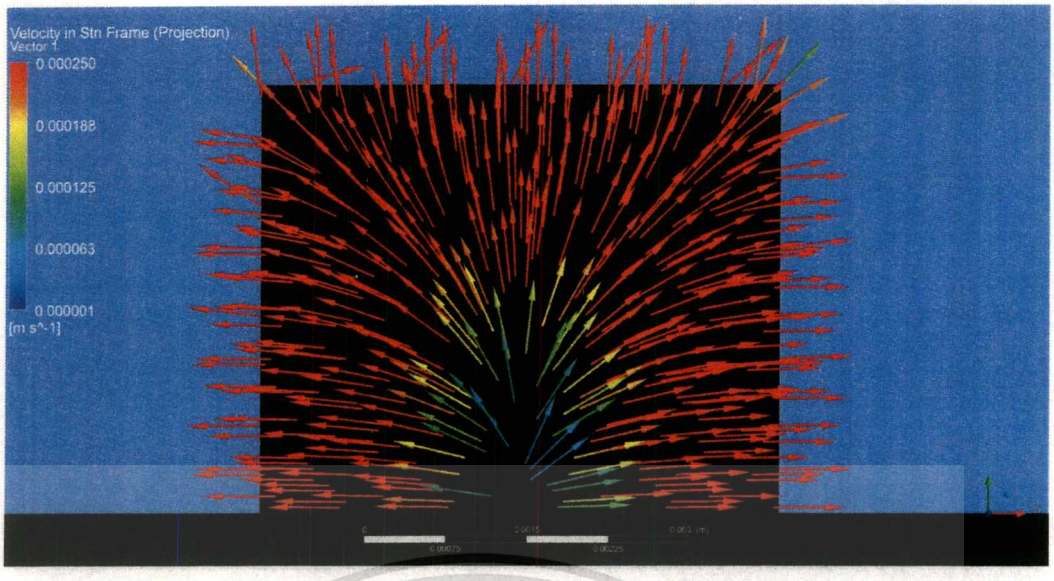

Figure 5.21 Vector of velocity inside the specimen at 16,000 s debinded with heating rate of 0.6 °C/min

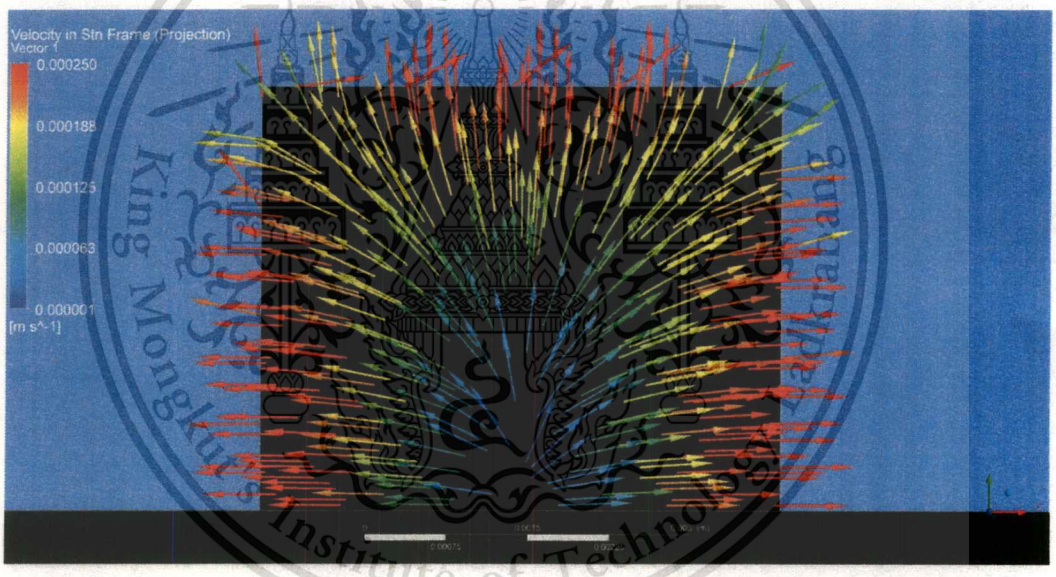

Figure 5.22 Vector of velocity inside the specimen at 16,000 s debinded with heating rate of 0.8 °C/min

5.4 Proposed heating profile for model of thermal debinding

The thermal debinding was adopted into simulation model based on CFD. The general propose software was ustilised by developing the thermal degradation model and other necessary code. All code were added into the general flow model of Ansys fluent. The model was established and validated experimentally. Then, The next step of the development was to find out safe heating profile that prevent damage of the specimen.

The model was proposed with the damage parameter which was pressure maximum in the specimen. Based on model of thermal debinding with 0.2 °C/min of heating rate, The pressure was observed that was maximised at 2,201.0 Pa. The pressure for the new model had to be controlled at value lower than 2,201.0 Pa. However, the maximum pressure for thermal bebinding was discovered that occurred in the early stage of debinding or in low temperature region. The high heating rate could be applied after the debinding had passed the point of maximum pressure.

The more sophisitcate heating profile was proposed. It consisted of two heating rates. The first should be less than 0.2 °C/min and the second was 1.0 °C/min as showed in figure 5.23. The history of specimen weight were plotted VS debinding time. The mass in specimen reduced rapidly when the heating rate was changed. To compare debinding time percentages of mass at 10% was considered that described in section 4.1. The new heating profiles could reduce debinding time from 100,000 s to 55,000s. The recommendation for the first heating rate could be used until internal pressure reduce from the maximum corresponding to debinding time of 40,240s. Then, the second heating was used to complete the debinding step.

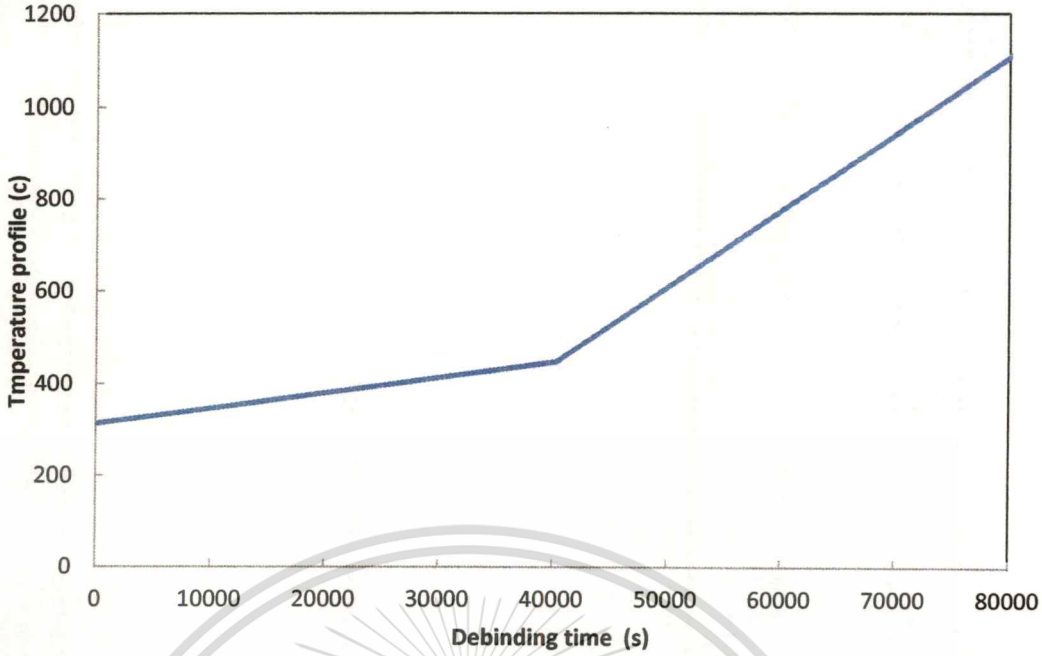

Figure 5.23 newly proposed heating profiles

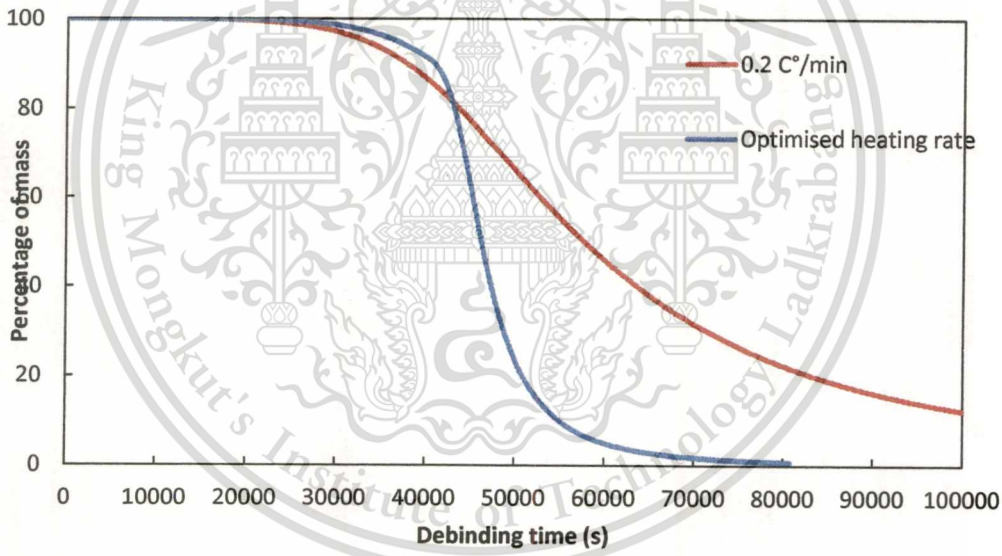

figure 5.24 Percentage of mass of the two heating profiles

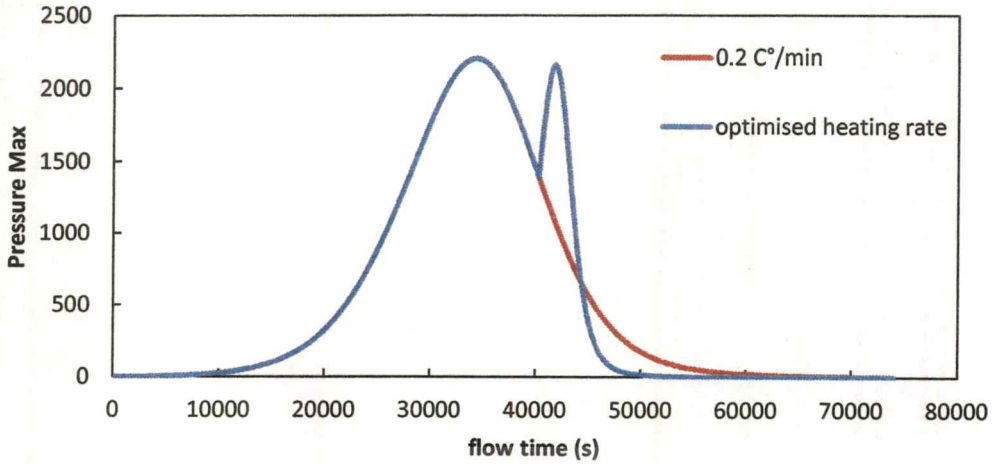

Figure 5.25 Maximum pressure in specimen of the two heating profiles

Chapter 6

CONCLUDSION AND SUGGESTIONS

6.1 Conclusions

Thermal debinding was the time-consuming step in Metal injection moulding process. There were many physical phenomena inside the specimen during this step. To capture the physic, heat and mass transfer in porous media were studied such as polymer degradation, multiphase flow, and darcy's law. Moreover, the model was developed based on CFD commercial software, Ansys Fluent. The computer code was added to perform and improve the general flow model to be thermal debinding model.

The model of thermal debinding was proposed. The thermo gravimetric data were employed to obtain the material parameters to complete the model of thermal debinding. The weight of polymeric binder and generation of volatile vapour was evaluated. Under the scope of this study, the numerical model is able to give the idea of pressure rise when compare with experimental resulted in the low temperature region up to 200 °C. This region was important to thermal debinding because deflects frequently occur in low temperature as the polymeric binder degrades rapidly. The weight of polymer inside specimen should affect to removal rate. From parametric analysis, there were a few variable could effect to the model. Activation energy and reaction order gave a widely variation of weight remain in specimen during thermal debinding.

The newly proposed model was developed. Heating profiles used for thermal debinding could be kept as low as possible to avoid any deflection. However, high heating rate such as 0.4, 0.6, 0.8 °C/min were examined. There were distortions on shape of specimen. Some hole were found inside the specimen from debinding with high heating rate. The model of thermal debinding showed good reasonable results to describe to cause of damage on specimen. The pressure inside specimen could be carefully controlled. The generation of degraded vapour in porous specimen increased the internal pressure which depended on the specimen temperature. Therefore, the proper heating rate was proposed from low heating rate. The initial heating rate should be kept below 0.2 °C/min. After the maximum pressure point, the higher heating rate could be used.

6.2 Suggestions

There are some suggestions to the work for further study as follow:

1. The model could be used for other injection condition. Different polymeric binder could be used, the mass source term (equation 3.13) should be modified for kinetic parameters from TGA testing of different polymer used.

2. The velocity of Air flow could be increased in order to improve heat transfer. Specimen could be heated with greater heat transfer because increment of velocity could lead to gain temperature gradient. As a result, the difference of specimen's temperature should be reduced when the velocity increased

REFFERENCE

1. Barone, M.R., Ulicny, J.C. 1990. "Liquid-phase transport during removal of organic binders in injection-molded ceramics." **Journal of the American ceramic society**. 73: 3323-3333.
2. Calvert, P., Cima, M., 1990. "Theoretical models for binder burnout." **Journal of American ceramic society**. 73: 575-579.
3. Chan, J.H., Balke, J.H. 1997. "The thermal degradation kinetics of polypropylene: part II. Thermogravimetric analyses." **Polymer Degradation and Stability**. 57: 135–149.
4. German, R.M., 1981. "Porosity and particle size effects on the gas flow characteristice of porous metal." **Powder Technology**. 30: 81-86.
5. Khoong, L.E. , Lam, Y.C., Chai, J.C., Ma, J., Jiang, L. 2010. "Modelling of mass transfers in a porous green compact with two-component binder during thermal debinding." **Chemical Engineering Science**. 64, 2837-2850.
6. Lam, Y.C., Shengjie, Y., Yu, S.C.M., Tam, K.C. 2000. "Simulation of polymer removal from a powder injection moulding compact by thermal debinding." **Metallurgical and Materials Transactions A**. 31A: 2598-2606.
7. Lewis, J.A., Galler, M.A., 1996. "Computer simulation of binder removal from 2-D and 3-d model Particulate Bodies." **Journal of American Ceramic Society**. 79: 1377-1388.
8. Maximenko, A., Van Der Biest, O., 1998. "Finite element modeling of binder removal from ceramic mouldings." **Journal of the European Ceramic Society**. 79: 1001-1009.
9. Sachanandani, M. R., Lombardo, S.J., 2011. "Effect of green body size and heating rate on failure during thermal debinding and on the debinding cycle time." **Journal of ceramic processing research**. 12 no2: 115-121.
10. Wenjea, T.J., Chung, K.H. 1999. "Cracking defect and porosity evolution during thermal debinding in ceramic injection molding." **Ceramics International**. 25: 461-466.
11. West, A.C., Lombado, S. J., 1998. "The role of thermal and transport properties on the binder burnout of injection-molded ceramic components." **Chemecal engineering Journal**. 71: 243-252.